European Journal of Medicinal Chemistry 281 (2025) 117037

Contents lists available at ScienceDirect

European Journal of Medicinal Chemistry

journal homepage: www.elsevier.com/locate/ejmech

Research paper

Development of selective sigma-1 receptor ligands with antiallodynic activity: A focus on piperidine and piperazine scaffolds

Giuseppe Cosentino [a], Maria Dichiara [a,**], Francesca Alessandra Ambrosio [b], Claudia Giovanna Leotta [d], Giosuè Costa [b,c], Francesca Procopio [b], Giuliana Costanzo [a], Alessandro Raffa [a], Antonia Artacho-Cordón [e], M. Carmen Ruiz-Cantero [e], Lorella Pasquinucci [a], Agostino Marrazzo [a], Giovanni Mario Pitari [d], Enrique J. Cobos [e], Stefano Alcaro [b,c], Emanuele Amata [a,*]

[a] University of Catania, Dipartimento di Scienze del Farmaco e della Salute, Viale A. Doria 6, 95125, Catania, Italy
[b] Dipartimento di Scienze della Salute, Università "Magna Græcia" di Catanzaro, Campus "S. Venuta", 88100, Catanzaro, Italy
[c] Net4Science Academic Spin-Off, Università "Magna Græcia" di Catanzaro, Campus "S. Venuta", 88100, Catanzaro, Italy
[d] Vera Salus Ricerca S.r.l., Via Sigmund Freud 62/B, 96100, Siracusa, Italy
[e] Departamento de Farmacología e Instituto de Neurociencias, Facultad de Medicina, Universitad de Granada e Instituto de Investigación Biosanitaria de Granada ibs. GRANADA, Avenida de la Investigación, 18016, Granada, Spain

ARTICLE INFO

Keywords:
Sigma-1 receptor antagonist
Pain
Analgesia
Molecular modeling

ABSTRACT

The design and synthesis of a series of piperidine and piperazine-based derivatives as selective sigma receptor (SR) ligands associated with analgesic activity, are the focus of this work. In this study, affinities at S1R and S2R were measured, and molecular modeling studies were performed to investigate the binding pose features. The most promising compounds were subjected to *in vitro* toxicity testing and subsequently screened for *in vivo* analgesic properties. Compounds **12a** (AD353) and **12c** (AD408) exhibited negligible *in vitro* cellular toxicity and high potency both in a model of capsaicin-induced allodynia and in PGE2-induced mechanical hyperalgesia. Functional activity experiments showed that S1R antagonism is needed for the effects of these compounds, since the effect was reversed by PRE-084 or absent in KO mice. In addition, **12a** exhibited a favorable pharmacokinetic profile, confirming its therapeutic value in treating allodynic conditions. Moreover, a computational model was developed in order to help the understanding about the mechanism of action of most active compounds.

1. Introduction

Neuropathic pain (NP) occurs due to a damage or disease impacting the peripheral or central somatosensory nervous system, affecting approximately 7–10 % of the global population [1,2]. Chronic NP is more prevalent in women (8 %) than in men (5.7 %), and it is more common in individuals over the age of 50 years (8.9 % *vs* 5.6 %) [3].

The complex pathophysiology of NP complicates effective treatment. Standard analgesics like non-steroidal anti-inflammatory drugs and opioids are ineffective, with chronic opioid use leading to dependence, tolerance, and constipation [4,5]. First-line treatment, including tricyclic antidepressant (TCAs), gabapentinoids, selective serotonin reuptake inhibitor (SSRIs), and serotonin–norepinephrine reuptake inhibitor (SNRIs), often require frequent replacement due to variable efficacy and side effects such as sedation, dizziness, and gait instability [6,7].

Sigma receptors (SR) – specifically sigma-1 receptor (S1R) and sigma-2 receptor (S2R) – are promising targets for NP treatment [8]. Notably, S1R expression is upregulated in the spinal cord of NP animal models, and knockout mice lacking S1R show reduced mechanical and thermal hypersensitivity after spinal cord injury (SCI) [9]. Additionally, S1R antagonists induce significant analgesia in NP model with fewer side effects, such as addiction and tolerance, compared to conventional therapies [10–13]. Unlike opioids, S1R antagonists do not affect normal sensory thresholds for mechanical and thermal stimuli, exerting anti-hypersensitivity effects – both antihyperalgesic and antiallodynic – in sensitized conditions [14]. S1R is expressed in both the peripheral and

* Corresponding author.
** Corresponding author.
E-mail addresses: maria.dichiara@unisi.it (M. Dichiara), eamata@unict.it (E. Amata).

https://doi.org/10.1016/j.ejmech.2024.117037
Received 13 September 2024; Received in revised form 5 November 2024; Accepted 5 November 2024
Available online 10 November 2024

central nervous systems, primarily in the endoplasmic reticulum (ER) membrane at the ER–mitochondria interface [15]. Upon activation, S1R enhances intracellular Ca^{++} levels and increases *N*-methyl-D-aspartate receptor (NMDAr) sensitivity, leading to greater Na^{+} and Ca^{++} influx [16–18]. This activates the extracellular signal-regulated kinases (ERK) 1/2 pathway, boosting NMDAr transcription and contributing to neuronal hyperexcitability and excitotoxicity [19–22]. Also, S1R knockout mice show reduced expression of TNF-α and IL-1β, along with decreased activation of NMDA and ERK 1/2 receptors in the spinal dorsal horn (SDH) [23,24]. In SCI models, microglia cells (MC) – which act as macrophage-like cells in the central nervous system (CNS) and regulate neuronal activity – become activated and release high levels of IL-1β, IL-18, and TNF-α, exacerbating NP [25–29]. The use of S1R ligands has showed neuroprotective effects by preventing the NMDA-mediated excitotoxicity and reactive oxygen species (ROS)-induced oxidative stress and inhibiting proinflammatory cytokine production [30,31]. Notably, S1R agonists as afobazole and (+)-pentazocine (PTZ) reduce the release of inflammatory cytokines in activated primary microglia cultures, while the S1R antagonist SN79 reduces cytokines expression upregulation after microglia activation [32–37]. However, the precise mechanisms by which S1R regulate the microglia activity remain to be fully elucidated [38].

S2R – recently identified as transmembrane protein 97 (TMEM97) – is a four-domain transmembrane receptor found in various degeneration-prone cell types, including neurons. S2R plays a crucial role in regulating several cellular functions, including cholesterol biosynthesis and trafficking, membrane trafficking, autophagy, lipid membrane-bound protein transport, and the stabilization of receptors at the cell surface [39]. S2R is highly expressed in human nociceptors and satellite glial cells, making it a promising target for NP treatment [40]. S2R agonists have been reported for their effects on mechanical hypersensitivity in the spared nerve injury (SNI) model with higher potency than gabapentin [41]. The anti-allodynia effect is likely mediated by alterations in transcriptional and regulatory processes within neurons. Notably, this effect intensified over 24h and persisted for up to 48h after administration [41,42]. On the other hand, S2R antagonists – such as SAS-0132 and JVW 1009 – are reported to provide neuroprotection against amyloid precursor protein-mediated neurodegeneration *in vitro*, improve cognitive performance, and reduce neuroinflammation *in vivo* [43].

In recent years, some analogs have been synthesized by many research groups for different therapeutic purposes [44–46]. Among these, piperazine and piperidine derivatives possess high SR affinity (Fig. 1). S1R antagonists containing basic piperazine like BD-1063 (**1**), and AV1066 (**2**) have been extensively studied in NP models proving analgesic effects [47,48]. Déciga-Campos et al. developed a benzyl derivative – *N*-(1-benzylpiperidin-4-yl)-4-fluorobenzamide (LMH-2) – which displayed S1R affinity and selectivity, dose-dependent antihyperalgesic and antiallodynic effects *in vivo* [49,50].

Conversely, S1R agonists like Cutamesine (**3**), have been reported for their implications in modulating neurological and psychiatric disorders [51,52]. SR ligands including a piperidine scaffold in their structure – Donepezil (**4**) and 4-IPB (**5**) – are reported for their neuroprotective and antidepressant effects in several models, including a zebrafish model of synaptic degeneration and a mouse model of amyloid-induced memory impairments [53–56].

Inspired by this and considering our interest in exploring the piperazine/piperidine nucleus [57,58], we designed, synthesized, and evaluated a series of derivatives containing these core moieties. The design of these compounds also contemplated the presence of a phenylacetate/phenylacetamide moiety to examine its impact on SR affinity. Indeed, when designing ligands for SR, the choice between ester and amide functionalities can significantly impact the ligand's affinity, selectivity, stability, and pharmacokinetic properties [59]. Beside the stronger or lower hydrogen bonding capabilities which lead to higher or minor affinity respectively, the rigidity of the amide bond or the flexibility of esters might be beneficial in certain contexts [60]. The planar structure of the amide bond restricts rotational freedom, potentially maintaining an optimal binding conformation for SR interaction. In contrast, the ester bond's greater rotational flexibility can either enhance or diminish binding, depending on the receptor environment and overall molecular design. For this purpose, a molecular modeling analysis was also conducted to thoroughly assess the binding modes of the ligands within the SR pockets. Finally, the most interesting compounds were tested for their *in vitro* cytotoxicity and *in vivo* antiallodynic activity, along with a preliminary pharmacokinetic investigation.

2. Results and discussion

2.1. Chemistry

Scheme 1 illustrates the overall process for the synthesis of the piperidine and piperazine derivatives developed in this work. Starting from the commercially available α-bromophenylacetic acid (**6**), amide **7a** has been obtained by two steps process involving the acyl chloride formation before the addition of diethylamine; whereas, ester **7b** has been obtained by Fischer esterification conditions.

Piperazine intermediates **9b**,**d** have been prepared by reductive amination of the appropriate aldehyde derivative in the presence of *N*-Boc-piperazine **8a** and $NaBH_3CN$ as reductant. Nucleophilic substitution of (2-bromoethyl)benzene and (3-bromopropyl)benzene, respectively, at **8b** resulted in piperidine derivatives **9a**,**c**. Removal of *N*-Boc

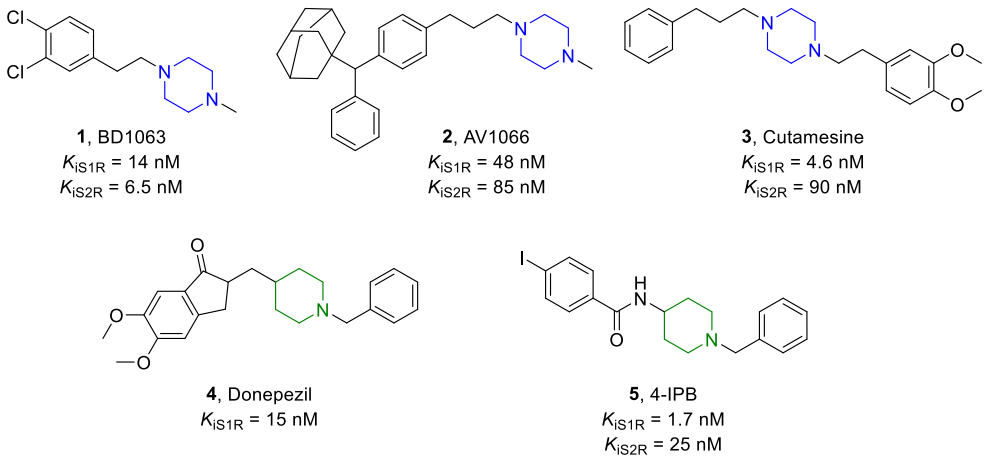

Fig. 1. Structure and affinities of S1R piperazine and piperidine based ligands.

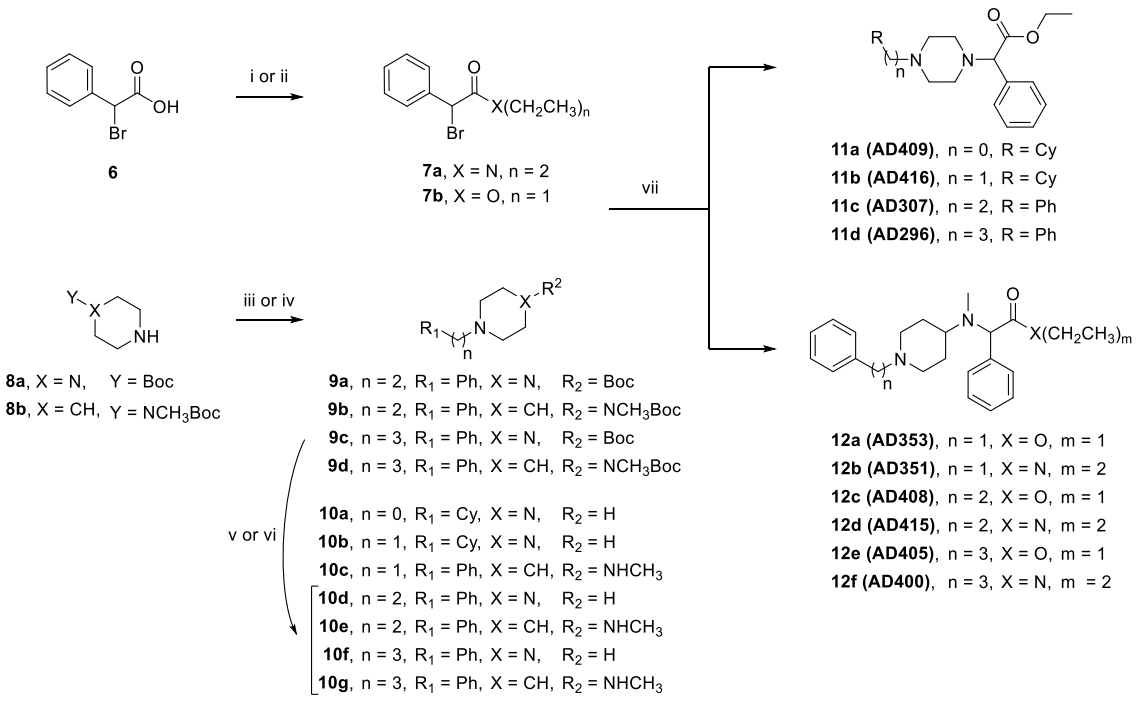

Scheme 1. Synthesis of piperazine and piperidine derivatives SR ligands. *Reagents and conditions*: (i) 1. $SOCl_2$, reflux, 3h, 2. CH_2Cl_2, $NH(CH_3CH_2)_2$, DIPEA, rt, on; (ii) EtOH, H_2SO_4, 65 °C, on; (iii) CH_3OH, CH_3COOH, $NaBH_3CN$, opportune phenylaldehyde, rt, on; (iv) THF, opportune phenylbromide, TEA, 65 °C, on; (v) HCl 4 M in dioxane, rt, 7h; (vi) TFA, CH_2Cl_2, rt, on; (vii) base, CH_3CN rt to reflux, 1h to on.

protecting group using HCl in dioxane or TFA in CH_2Cl_2 gave the corresponding free amines **10d–g**. Nucleophilic substitution of **7b** with commercially available piperazines **9a**,**b** or intermediates compounds **10d**,**f** gave the first set of final derivatives **11a**,**d**. Conversely, nucleophilic substitution of **7a**,**b** with commercially available piperidine **10c** or intermediates **10d**,**g** gave the final derivatives **12a**,**f**.

All compounds were prepared as racemic mixtures and utilized without separating into individual enantiomers for further pharmacological investigations.

2.2. *In vitro binding assays and structure-affinity relationship analysis*

All the synthesized compounds were evaluated for affinity at both S1R and S2R through radioligand binding assays using [^{3}H]-(+)-PTZ and [^{3}H]-1,3-di-(2-tolyl)guanidine (DTG) as radioligands for S1R and S2R, respectively. Nonspecific binding for S1R was measured in the presence of 10 μM unlabeled PTZ and in the presence of 10 μM unlabeled DTG for S2R assays. Moreover, since a selective S2R radioligand is not available, [^{3}H]DTG was used in the presence of an excess of PTZ to mask the S1R sites. The results are summarized in Table 1.

In the first set of compounds, we retained piperazine as the basic moiety, which is a crucial structural element for SR affinity [61]. While the piperazine derivatives interact slightly more strongly with S1R than with S2R, the length of the alkyl linker doesn't have a noticeable impact on their affinity. Compound **11a** (AD409), having a cyclohexyl substituent, exhibits low S1R affinity in the three-digit nanomolar range. However, increasing the chain length by incorporating a methyl cyclohexyl group as in compound **11b** (AD416), results in a complete loss of binding ability to both receptors. Compounds **11c** (AD307) and **11d** (AD296) showed a similar affinity profile in the hundred nanomolar range for both subtypes. Replacing the piperazine ring with a *N*-methyl piperidine yielded derivatives with strong to moderate affinity for S1R, with K_i values ranging from 0.54 to 108 nM, and different ranges of selectivity over S2R. The different structural features, particularly the nitrogen-nitrogen distance and the flexibility of the ring, play a crucial role in determining the affinity and activity of ligands at SRs. Although

Table 1
SR binding assays for compounds **11a–d** and **12a–f**.

Cmpd	K_i (nM) ± SD[a]		
	S1R	S2R	S1R/S2R
11a	114 ± 37	232 ± 69	2.0
11b	>1000	>10,000	10
11c	268 ± 75	323 ± 22	1.2
11d	96 ± 16	134 ± 21	1.4
12a	0.54 ± 0.14	>10,000	>10,000
12b	65 ± 14	120 ± 21	1.9
12c	9.9 ± 0.75	>10,000	>10,000
12d	108 ± 16	73 ± 10	0.7
12e	11 ± 0.92	>1000	>1000
12f	83 ± 11	34 ± 3	0.4
PTZ[b]	4.3 ± 0.5	1465 ± 224	
DTG[b]	124 ± 19	18 ± 1	
Haloperidol[b]	2.6 ± 0.4	77 ± 18	
BD1063[b]	14 ± 2.7	204 ± 31	

[a] Each value is the mean ± SD of at least two experiments performed in duplicate.
[b] Taken from Ref. [12].

the positioning of the nitrogen atoms in piperazine is expected to allow for a more versatile interaction with SRs, the absence of a second nitrogen within the ring itself and the presence of a methyl group in *N*-methyl piperidine, lead to a more rigid structure which can tune the binding and selectivity for SRs. The benzyl derivative **12a** (AD353) demonstrated sub-nanomolar affinity for S1R and complete selectivity over S2R subtype. Extending the chain to two (**12c**, AD408) or three (**12e**, AD405) carbons resulted in a logarithmic decrease in S1R affinity, while maintaining S2R selectivity. Changing the phenylacetate with a phenylacetamide moiety, an inversion of the SR profile has been observed, with a preferential affinity for S2R. The only exception is compound **12b** (AD351), keeping higher affinity for S1R (K_i = 65 nM). Derivative **12d** (AD415), having a two-carbon chain length, showed lower S2R affinity (K_i = 73 nM) with respect to S1R (K_i = 108 nM).

Further elongation to the three-carbon chain resulted in compound **12f** (AD400) with lower S2R affinity (K_i = 34 nM) and improved selectivity over S1R.

Overall, the optimal compounds in terms of S1R affinity are those bearing the piperidine scaffold and the phenylacetate group. In-depth mechanistic studies provided valuable insights into the binding interactions between the ligands and SRs. Building on these findings, we chose to explore the effects of compounds **12a** and **12c** further through additional *in silico*, *in vitro*, and *in vivo* models.

2.3. Molecular modeling

Molecular modeling was employed to investigate the binding modes of piperazine and piperidine derivatives on SRs considering all the stereoisomers. Regarding the SR1, the docking simulations revealed that all the synthesized compounds, except for the **12d** derivative, were oriented within the S1R binding site with the protonated nitrogen in the anionic site engaging Glu172 in a salt bridge and, in some cases, in an additional hydrogen bond (Table S1). Moreover, the protonated nitrogen established a cation-π interaction with Phe107 in front of the Glu172 anionic site in almost all derivatives, except for **12d** and **12f** derivates. The phenyl alkyl chain of these compounds was accommodated in the secondary hydrophobic pocket, delineated by Asp126, Phe107, Val152, Phe133, Trp164, Glu135, Val162, His154, Trp89, and Ser117, which is 2.5–3.9 Å away from the Glu172 anionic site and able to tolerate bulky groups, in agreement with Glennon's pharmacophoric model [62]. Here, the compounds were involved in van der Waals interactions. Some of the derivatives, especially the most active compounds **12a**, **12c** (Fig. 2), and **12e**, showed π-π interactions with Trp89, Phe133, and Trp164. These π-π interactions may justify the higher binding affinity of compounds **12a**, **12c** and **12e**, as highlighted by their better K_i values. In fact, comparing compound **12a** with compound **11b** – where the phenyl moiety is substituted with an aliphatic cyclohexyl – the π-π interactions were lost, as reported in Table S1 and the K_i get worst. Moreover, superimposing the binding modes of piperidine and piperazine derivatives reveals that – although their pharmacophoric features are similar – piperidine compounds can form π-π interactions with hydrophobic residues like Trp89, Phe133, and Trp164. In contrast, piperazine derivatives cannot establish these interactions, contributing to the observed differences in activity.

Moreover, the phenylacetate moiety was oriented in the primary hydrophobic pocket surrounded by Met93, Leu95, Tyr206, Ile178, Val84, Tyr103, Leu182, and Ala185, and is 6–10 Å away from Glu172. Almost all the *R* enantiomers established a hydrogen bond with Thr181, whereas the *S* enantiomers often engaged in π-π stacking with Tyr103. Further analysis of compound **12d** reveals that its distinct orientation – due to the increased bulk of the diethylamide group and the longer phenyl alkyl moiety – does not significantly impact its molecular recognition of the S1R. Notably, key interactions, including the salt bridge and hydrogen bond with Glu172, as well as the cation-π interaction, remain intact (see Table S1).

The same docking analysis performed on SR2 revealed that all the synthesized compounds were oriented within the binding site with the protonated nitrogen engaging Asp29 in a salt bridge and, in some cases, in a cation-π with Tyr150. The phenyl alkyl chain of these compounds was involved in hydrophobic interactions with the residues lying in the receptor binding cavity; furthermore, some of the derivates established a π-π interaction with Tyr50 (Supporting Information, Table S2). Considering the higher affinity of compounds **12a** and **12c** versus S1R, the thermodynamics profile against both SR1 and SR2 was further inspected using the eMBrAcE calculation tool that estimates the binding free energy for each ligand at molecular mechanic level [63]. The eMBrAcE results highlighted a better interaction energy between the SR1 and each ligand, compared to SR2, in agreement with experimental data (Table 2). By investigating the single contributions of the E energy components, the electrostatic term resulted in the driven force in the binding process (Table 3) and potentially responsible for the S1R selectivity.

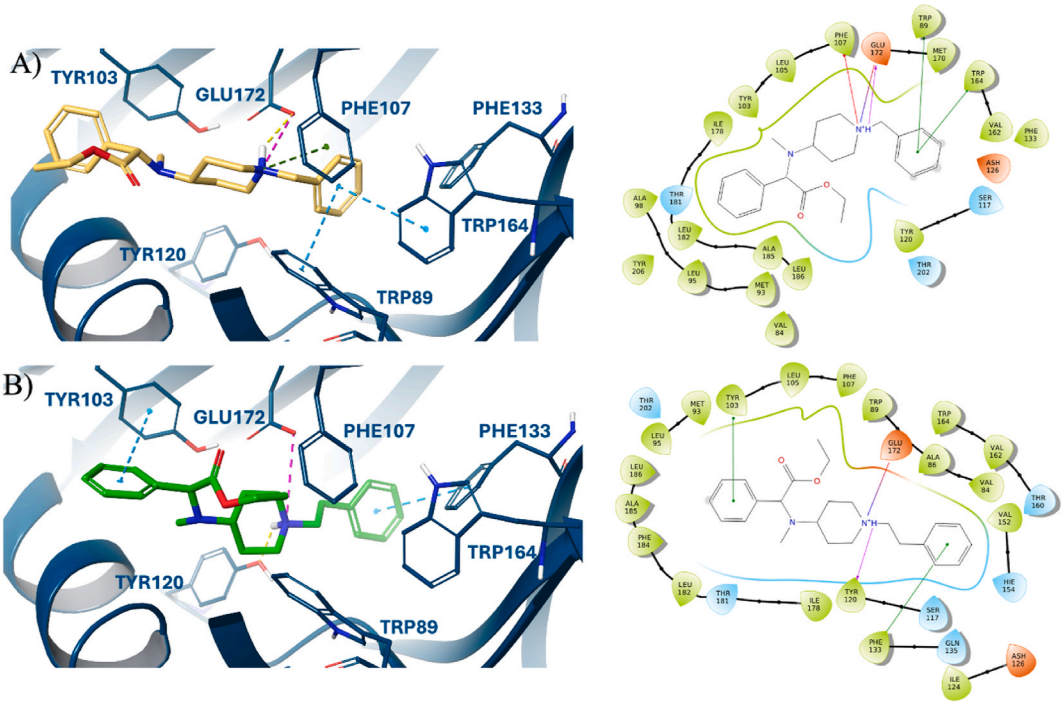

Fig. 2. 3D and 2D representation of the best scoring enantiomer of (A) **12a** and (B) **12c** docked in the binding pocket of the S1R. In the 3D representation ligands are shown as yellow and green sticks, respectively. The S1R is shown as a blue cartoon, and the amino acids engaged in pivotal contacts with the ligands are represented as blue carbon sticks. Salt bridges, π–π stacking, π–cation and hydrogen bonds interactions are, respectively, represented by magenta, azure, green, and yellow dashed lines. In the 2D representation salt bridges, π–π stacking, π–cation and hydrogen bonds interactions are represented as red-blue, green, red and magenta lines, respectively.

Table 2
eMBrAcE energy (E) values and their single contributions, expressed as electrostatic (EElec) and van der Waals (EvdW), calculated for **12a** and **12c** complexed with S1R and S2R.

Compound		S1R			S2R		
		E	E_{VdW}	E_{Elec}	E	E_{VdW}	E_{Elec}
R	**12a**	−718.59	−181.96	−536.64	−529.60	−192.13	−337.47
S		−780.04	−191.55	−588.49	−590.66	−166.71	−423.95
R	**12c**	−766.02	−184.26	−581.76	−620.83	−221.12	−399.71
S		−696.11	−190.76	−505.35	−627.83	−191.33	−436.50

*The thermodynamic values are reported in KJ/mol.

Table 3
Preliminary ADMET characterization for compound **12a**.

	Medium	
chemical stability $t_{1/2}$ (min)[a]	Phosphate buffer pH 7.4	95.4
water solubility (mg/mL)[a]		1.87
logP[a]	*n*-octanol/water	1.79
logD[pH 7.4][a]	*n*-octanol/PBS	1.72
hERG (μM)		1.6

[a] Each value is the mean ± SD of three experiments performed in triplicate.

2.4. Safety assessment in vitro

Possible negative impacts on CNS cell biology by compounds **12a** and **12c** were examined in the human microglial clone 3 (HMC3) cell line with the acridine orange staining assay [64]. S1R agonist PTZ and S1R antagonist BD-1063 were employed as reference compounds. At tested concentrations (0.1 μM–30 μM), compounds **12a** and **12c** did not perturb HMC3 cell proliferation, as compared to the vehicle control (Fig. 3). PTZ and BD-1063 (0.1 μM–30 μM) also did not alter HMC3 cell proliferation, indicating that targeting S1R is relatively safe under these experimental conditions. In agreement, **12a** failed to induce overt antiproliferation and cytotoxicity in human skin fibroblast WS1 cells, employed as a general model of systemic toxicity (Supporting Information, Fig. S1).

2.5. In vivo functional profile: capsaicin-induced mechanical hypersensitivity and PGE2-induced mechanical hyperalgesia

We tested the effect of compounds **12a** and **12c** in capsaicin-induced mechanical hypersensitivity (allodynia) in mice (Fig. 4). The increase in pain sensitivity in the area surrounding capsaicin injection results from central sensitization, and this process plays a pivotal role in chronic pain development and maintenance [65]. Capsaicin-induced mechanical hypersensitivity has been used to study drug effects in central sensitization in both humans and rodents [66,67]. In particular, this behavioral model has been previously employed to evaluate the S1R functional profile of new compounds (including clinical candidates) since compounds that act as antagonists at S1R can reduce sensory hypersensitivity, whereas compounds that act as agonists at S1R reverse the effects of the former [66,68,69]. S1RA (5–30 mg/kg, s.c.), used as a control standard S1R antagonist, induced a dose-dependent and full reversal of capsaicin-induced allodynia, as previously described [66,69]. Similar to the effect of the standard S1RA, compounds **12a** (2–10 mg/kg, s.c.) and **12c** (AD408) (1–10 mg/kg, s.c.) also induced dose-dependent and full reversal of capsaicin-induced allodynia at the maximum doses tested, yielding significant antiallodynic effects from the dose of 5 mg/kg for **12a** and 2 mg/kg for **12c** (Fig. 4A). We then tested the *in vivo* effects of the association of these compounds with PRE-084 (32 mg/kg, s.c.), a prototypic S1R agonist. We selected drug doses that induced the maximum antiallodynic effect of each compound (i.e. S1RA 30 mg/kg, **12a** 10 mg/kg, and **12c** 10 mg/kg). The administration of PRE-084 fully reversed the antiallodynic effect of S1RA (Fig. 4B), as previously reported [66,69]. Importantly, administration of PRE-084 was also able to significantly reverse the effect of the other two experimental compounds. These results indicate that S1R antagonism is essential for the effect of these compounds on mechanical hypersensitivity (Fig. 4B).

We also tested the effect of two of our compounds in PGE2-induced mechanical hyperalgesia. The intraplantar (i.pl.) administration of PGE2 (0.5 nmol) to WT mice induced a marked decrease in struggle latency of the injected paw to mechanic stimulation, in comparison to saline-injected controls, denoting the development of mechanical hyperalgesia (Fig. 5A). The systemic (subcutaneous, s.c.) administration of the prototypic S1R antagonist S1RA (60 mg/kg) or the compounds **12a** (10 mg/kg) and **12c** (10 mg/kg) induced an increase in the response latency in PGE2-sensitized WT mice, reaching values similar to control animals (i.e. a full antihyperalgesic effect) and this effect was fully reversed by PRE-084 (32 mg/kg, s.c.) (Fig. 5A). We also tested the effect of PGE2 in S1R KO mice. This algogenic chemical induced a robust decrease in the response latency to mechanical stimulation in KO mice (Fig. 5B), and to a similar extent than in WT mice (compare Fig. 5A and B). This apparent discrepancy between the abolishment of PGE2 mechanical hypersensitivity in WT treated with S1R antagonists and the normal development of hyperalgesia in S1R KO mice has been previously reported [70,71]. In fact, this is not the only pain model with conflicting results of this type in S1R research, as there are reported discrepancies between the effects of

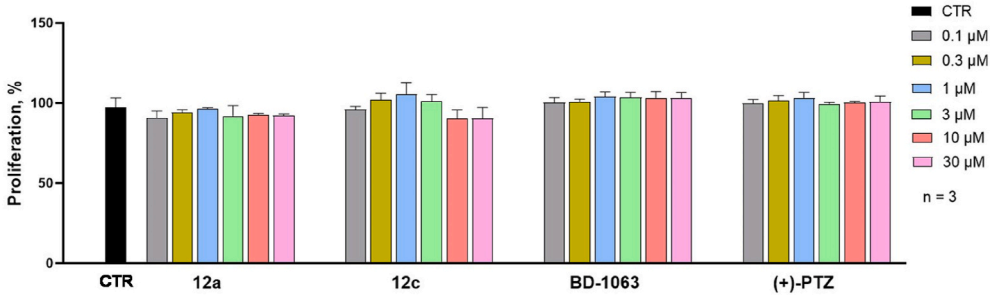

Fig. 3. Antiproliferative effects of **12a**, **12c**, BD-1063 and PTZ on human microglial HMC3 cells. Data represents the percentage of proliferation with respect to the vehicle DMSO control (CTR). Values are expressed as mean ± SEM of three independent experiments, each conducted in triplicate. Statistical analysis was performed using one-way ANOVA.

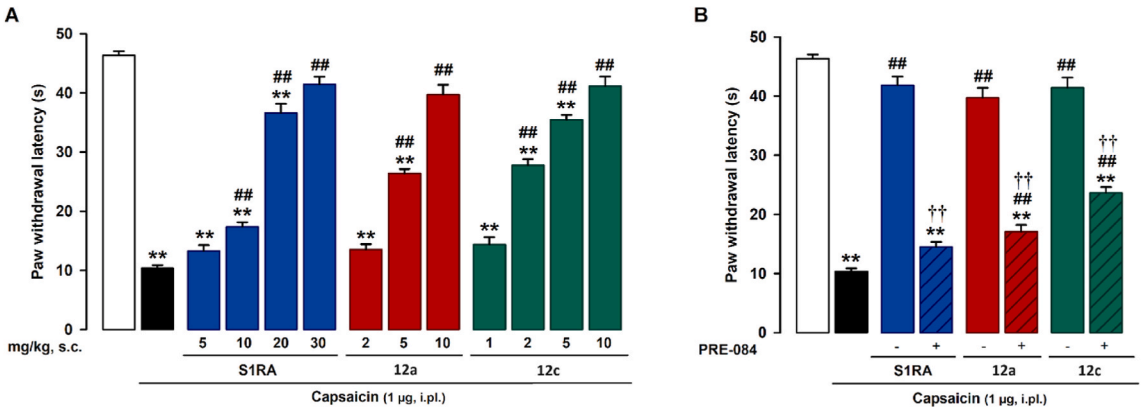

Fig. 4. Reduction of capsaicin-induced mechanical allodynia by the systemic administration of S1RA, **12a** and **12c**, and contribution of S1R to their effects. The results represent the latency to paw withdrawal in response to a punctate mechanical stimulus of 0.5 g in mice. (A) Dose dependency of the antiallodynic effects of the s.c. administration of S1RA, **12a** and **12c** in wild-type mice. (B) Effects of the S1RA (30 mg/kg), **12a** (10 mg/kg) or **12c** (10 mg/kg), tested alone and associated with the S1R agonist PRE-084 (32 mg/kg) in wild-type mice. Each bar and vertical line are the mean ± SEM of the values obtained in 6 animals: **p < 0.01 vs non-sensitized animals treated with the solvent of the drugs (white bar); ##p < 0.01 vs capsaicin-injected mice (black bar); ††p < 0.01 vs selected doses of each compound associated with PRE-084 (one-way ANOVA followed by Bonferroni test).

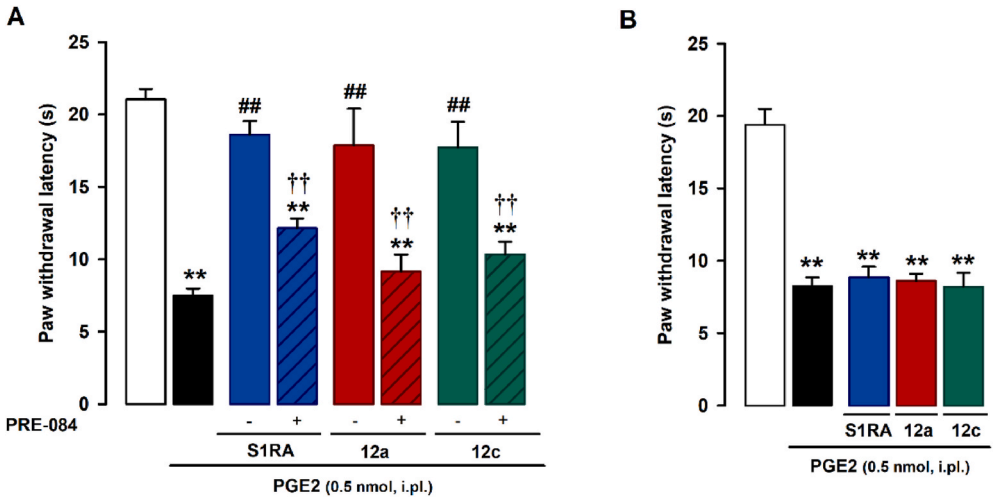

Fig. 5. Reduction of PGE2-induced mechanical hyperalgesia by the systemic administration of S1RA, **12a** and **12c**, and contribution of S1R to their effects. The results represent the latency to struggle response evoked by a blunt mechanical stimulus of 100 g in mice. (A) Effect of the s.c. administration of the S1R antagonist S1RA (60 mg/kg) and the compounds **12a** (10 mg/kg) and **12c** (10 mg/kg) alone or in combination with the s.c. administration of the S1R agonist PRE-084 (32 mg/kg) on mechanical hyperalgesia induced by PGE2 in wild-type mice. (B) Effect of the s.c. administration of compounds **12a** (10 mg/kg) and **12c** (10 mg/kg) on mechanical hyperalgesia induced by PGE2 in S1R knockout mice. Each bar and vertical line are the mean ± SEM of the values obtained in 6–8 animals: **p < 0.01 *vs* non-sensitized animals treated with the solvent of the drugs (white bar); ##p < 0.01 vs PGE2-injected mice (black bar); ††p < 0.01 vs compound associated with PRE-084 (one-way ANOVA followed by Bonferroni test).

pharmacological and genetic inhibition of S1R also in inflammatory and NP models [72,73], which have been attributed to compensatory mechanisms in pain pathways of S1R knockout mice [71–73]. Regardless of the exact mechanism responsible for these discrepancies, S1R KO mice can be used to test the selectivity of the effect of S1R compounds, as the mutant animals lack the putative target of the drugs under study. Therefore, it would be expected that if these drugs were truly selective, they would lose their effect in S1R KO animals. Consistent with this reasoning, we found that not only the prototypic S1R antagonist S1RA (60 mg/kg) completely lost its antihyperalgesic effect in S1R KO animals, but also the compounds **12a** (10 mg/kg) and **12c** (10 mg/kg) (Fig. 5B).

However, since we have not evaluated compounds **12a** and **12c** against a panel of drug targets, we cannot ensure their selectivity based solely on existing literature studies [74–76]. Indeed, the compounds under investigation possess pharmacophoric features that align with established classes of agents such as the acetylcholinesterase (AChE) modulator donepezil. Consequently, we cannot rule out potential effects related with the modulation of other targets including AChE. Nevertheless, our results on capsaicin-induced mechanical allodynia and PGE2-induced hyperalgesia, in which the effects of both compounds were absent in mice lacking sigma-1 receptors and/or reversed by sigma-1 agonism in wild-type animals, suggest that sigma-1 receptors are involved in the *in vivo* effects of the drugs tested. Regarding the mechanism involved in these effects, it is worth mentioning that the sensitization of the nociceptive system by either capsaicin or PGE2 is sustained by the activity of Transient Receptor Potential Vanilloid 1 (TRPV1) expressing nociceptors [70,71,77]. It is known that S1R can bind to TRPV1, and we reported that S1R antagonism could decrease the activity of TRPV1-expressing neurons [70], which might be involved in the effects induced by **12a** and **12c**.

Altogether, our results suggest that **12a** and **12c** are S1R antagonists and could have therapeutic value to treat both mechanical allodynia and hyperalgesia.

2.6. Initial ADMET profile

The water solubility and chemical stability for compound **12a** were experimentally determined, while partition coefficients theoretically calculated (Table 3). Compound **12a** (free base) displayed a water solubility of 1.87 mg/mL at rt. The chemical stability was evaluated at 37 °C in an aqueous phosphate buffer (PBS) at pH 7.4 showing a general acceptable profile. Partition coefficients logP and logD[pH 7.4] were of 1.79 and 1.72, respectively, demonstrating moderate lipophilicity. This suggests that the compound is well-absorbed in biological systems, effectively balancing solubility in aqueous environments such as blood, with permeability through lipid membranes like cell membranes. Haloperidol has been used as reference compound, with a measured logP (4.03) and logD[pH 7.4] (3.99) similar to those reported in literature (see also Table S3) [78].

Compound **12a** was then evaluated *in silico* for its brain/plasma distribution using a statistical method previously developed by the authors [79]. As can be noted in Fig. 6, compound **12a** shows five computed descriptors in the BBB^{+} scenario (logP, logD[pH 7.4], polar surface area, ionization state, and hydrogen bond donor), and four in the BBB^{+}/BBB^{-} scenario (hydrogen bound acceptor, nitrogen atom count, oxygen atom count and nitrogen-oxygen count), indicating a good descriptors distribution for BBB permeation.

Given that inhibition of the potassium ion channel encoded by the human ether-a-go-go-related gene (hERG) was a recurring problem in previous S1R programs [80–82], we sought to investigate the potential of compound **12a** to block the hERG channel. Compound **12a** exhibited an IC_{50} of 1.6 μM (Supporting Information, Table S4) – higher than the standard compound verapamil (IC_{50} 0.27 μM) – which means a three-thousand-fold ratio *versus* its S1R affinity. It is thought that a 30-fold difference between the effective therapeutic plasma concentration and hERG IC_{50} may be sufficient to prevent the appearance of Torsades de Pointes associated with QT prolongation [83]. However, since the usual IC_{50} cut-off is 10 μM, the hERG inhibition of **12a** is an alert to be addressed in the future optimization of the series.

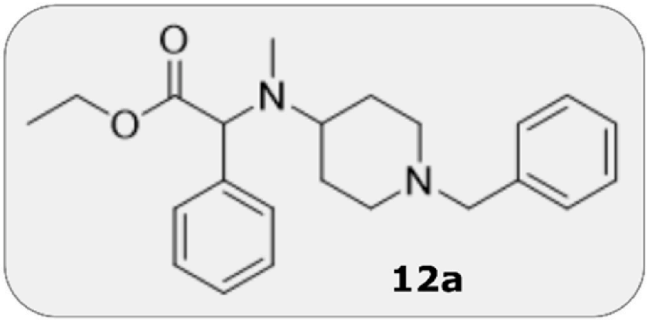

logP*	logD*	PSA	HBA
1.79	1.72	32.78	3
HBD	**NC**	**OC**	**NOC**
0	2	2	4
IS			
Basic			

*values obtained from experimental measurements.

descriptors in BBB^{+}

descriptors in BBB^{+}/BBB^{-}

descriptors in BBB^{-}

Fig. 6. BBB permeation descriptors distribution for compound **12a**.

3. Conclusion

In this study, 10 analogs containing the piperazine/piperidine nucleus were synthesized and evaluated for SR affinity in radioligand binding assays. The effect of adding phenylacetate or phenylacetamide groups on SR affinity was also thoroughly analyzed. Overall, the compounds with the highest S1R affinity are those featuring the *N*-methyl piperidine scaffold combined with the phenylacetate group. Probably, the ester bond enhances the SR binding allowing for more rotational flexibility with respect to the planar structure of the amide bond which restricts the rotational freedom. Mechanistic studies have provided insights into how the analogs interact with and activate, or fail to activate, the S1R, leading to hypotheses about their binding mechanisms. Compounds **12a** and **12c** emerged for their high affinity at S1R with selectivity in the thousand-fold range. Noteworthy, the thermodynamic simulation of best compounds' binding models carried out by eMBrAcE calculations, found agreement with the radioligand binding assays. Both compounds have been selected for further preliminary cytotoxicity *in vitro* tests – revealing to be well tolerated up to very high concentrations – and for *in vivo* pharmacological evaluation – exerting promising dose-dependent antiallodynic effects against capsaicin-induced pain in mice. The functional activity of compounds **12a** and **12c** was evaluated through *in vivo* experiments, showing that both compounds act as antagonists for the S1R. In fact, the effects on allodynia and hyperalgesia of these compounds are fully reversed by the S1R agonist PRE-084 or absent in KO mice. As representative example, compound **12a** has been further evaluated to assess its safety profile, including the blockade of hERG, an off-target related to cardiac toxicity, and preliminary pharmacokinetic profile. These results clearly suggest that **12a** and **12c** are S1R antagonists with potential therapeutic applications for both mechanical hyperalgesia and allodynia.

4. Materials and methods

4.1. General remarks

Reagent-grade chemicals were supplied by Merck (Milan, Italy) and used without further purification. All reactions involving air-sensitive reagents were conducted under nitrogen atmosphere. Flash chromatography purification was carried out using a Merck silica gel 60 (40–63 μm; 230–400 mesh) stationary phase. Electrospray ionization mass spectrometry (ESI-MS) spectra were performed by an Agilent 1100 series LC/MS spectrometer. NMR spectra (^{1}H and ^{13}C recorded at both 200 and 500 MHz) were acquired on VARIAN INOVA spectrometers using $CDCl_3$ as the solvent, with TMS as internal standard. Chemical shifts (δ) are reported in parts per million (ppm) and coupling constants (J) in Hertz (Hz). The following abbreviations denote the multiplicities: s = singlet, d = doublet, t = triplet, q = quartet, m = multiplet, br = broad. Microanalysis (C, H, N) performed on a Carlo Erba instrument model E1110, showed that all compounds tested, synthesized or purchased, reached a purity at least 95 %; all results were within ±0.4 % of the theoretical values. TLC monitoring was performed using 250 μm silica gel Merck 60 F_{254} coated aluminum plates, and the spots were visualized under UV light, permanganate or iodine chamber. Compounds nomenclature was generated using ChemBioDraw Ultra version 16.0.0.82.

4.2. Chemistry

4.2.1. General procedure amine preparation (procedure A)

To a solution of *tert*-butyl piperazine-1-carboxylate (**8a**, 1.00 eq) in CH_3OH (210 mM), the opportune aldehyde (1.00 eq) was added. The solution was cooled to 0 °C, then CH_3COOH (3 drops) and $NaBH_3CN$ (2.30 eq) were sequentially added. The reaction was stirred at rt on. After completion, the reaction mixture was concentrated *in vacuo*, the residue washed with a saturated solution of $NaHCO_3$ (1 x 10 mL) and extracted with EtOAc (2 x 10 mL). The organic layer was washed with brine (1 x 10 mL), dried over anhydrous Na_2SO_4, filtered and evaporated to dryness. The residue was purified via silica gel chromatography to obtain the desired product. Products synthesized according to this procedure are **9a** and **9c**.

4.2.2. General procedure amine preparation (procedure B)

tert-Butyl methyl(piperidin-4-yl)carbamate (**8b**, 1.00 eq) was dissolved in THF anhydrous (400 mM). Then, bromo-derivative (1.30 eq) and TEA (3.00 eq) were sequentially added at rt. The reaction was stirred at 65 °C on. After completion, the reaction mixture was concentrated *in vacuo*, the residue dissolved in EtOAc (30 mL), washed with a saturated solution of $NaHCO_3$ (1 x 10 mL), brine (1 x 10 mL), dried over anhydrous Na_2SO_4, filtered and evaporated to dryness. The residue was purified via silica gel chromatography to obtain the desired product. Products synthesized according to this procedure are **9b** and **9d**.

4.2.3. General procedure amine preparation (procedure C)

Compound **7b** (1.10 eq) was dissolved in CH_3CN anhydrous (200 mM). Then, the commercially available piperazine (1.00 eq) and K_2CO_3 (1.50 eq) were added at rt. The reaction mixture was stirred at 70 °C for 4 h. After completion, the mixture was concentrated *in vacuo*, the residue dissolved in EtOAc (20 mL), washed with a saturated solution of $NaHCO_3$ (1 x 10 mL), brine (1 x 10 mL), dried over anhydrous Na_2SO_4, filtered and evaporated to dryness. The residue was purified via silica gel chromatography to obtain the desired product. Products synthesized according to this procedure are **11a** and **11b**.

4.2.4. General procedure amine preparation (procedure D)

Boc-protected amine (1.00 eq) was dissolved in anhydrous CH_2Cl_2 (80 mM). The solution was cooled to 0 °C, then TFA (11.0 eq) was added dropwise. The reaction mixture was stirred at rt on. After completion, the reaction mixture was washed with NaOH 1 M (1 x 10 mL), extracted with CH_2Cl_2 (3 x 10 mL), washed with brine (1 x 10 mL), dried over anhydrous Na_2SO_4, filtered and evaporated to dryness. The residue (**10d** or **10f**) was then dissolved in CH_3CN anhydrous (100 mM), then **7b** (1.35 eq) and DIPEA (3.00 eq) were added at 0 °C. The reaction mixture was stirred at 0 °C for 1h. After completion of the transformation, the reaction mixture was quenched with a saturated solution of $NaHCO_3$ (10 mL), extracted with EtOAc (3 x 10 mL), washed with brine (1 x 15 mL), dried over anhydrous Na_2SO_4, filtered and evaporated to dryness. The residue was purified via silica gel chromatography to obtain the desired product. Products synthesized according to this procedure are **11c** and **11d**.

4.2.5. General procedure amine preparation (procedure E)

1-Benzyl-*N*-methylpiperidin-4-amine (**10c**, 1.00 eq) was dissolved in anhydrous CH_3CN (200 mM). Then, bromo-derivative (1.10 eq) and K_2CO_3 (152 mg, 1.10 mmol, 1.50 eq) were added at rt. The reaction mixture was stirred at 70 °C on. After completion, the reaction mixture was concentrated *in vacuo*, the residue dissolved in EtOAc (15 mL), was washed with a saturated solution of $NaHCO_3$ (1 x 5 mL), brine (1 x 5 mL), dried over anhydrous Na_2SO_4, filtered and evaporated to dryness. The residue was purified via silica gel chromatography to obtain the desired product. Products synthesized according to this procedure are **12a** and **12b.**

4.2.6. General procedure amine preparation (procedure F)

Boc-protected piperidine (**9b** or **9d**, 1.00 eq) was dissolved in a dried flask with anhydrous CH_2Cl_2 (100 mM) and HCl 4 M in dioxane (10.0 eq) was added dropwise in ice bath. The reaction mixture was stirred at rt for 7h followed by the removal of the solvents *in vacuo*. The residue (**10e** or **10f**) was then washed with anhydrous CH_2Cl_2 (3 x 1 mL), concentrated again and dissolved in anhydrous DMF (70 mM). At rt, bromo-derivative (**7a** or **7b**, 1.20 eq) and K_2CO_3 (3.00 eq) were sequentially added. The reaction mixture was stirred at 90 °C for 20h. After completion, the reaction mixture was concentrated *in vacuo*, the residue was dissolved in EtOAc (30 mL), washed with a saturated solution of $NaHCO_3$ (1 x 10 mL), brine (1 x 10 mL), dried over anhydrous Na_2SO_4, filtered and evaporated to dryness. The residue was purified via silica gel chromatography to obtain the desired product. Products synthesized according to this procedure are **12c**, **12d**, **12e** and **12f**.

4.2.7. General procedure for oxalate salts formation (procedure G)

For final compounds **11a** (AC339), **11b** (AC3), **11c** (AD307), **11d** (AD296) and **12a** (AC1) the pure product was dissolved in EtOAc and a solution of oxalic acid in EtOAc was added dropwise at 0 °C to obtain the desired product as oxalate salt.

4.2.8. General procedure for hydrochloride salts formation (procedure H)

For final compounds **12b** (AD351), **12c** (AD408), **12d** (AD415), **12e** (AD405) and **12f** (AD400), the pure product was dissolved in CH_2Cl_2 and a solution of 1.25 M HCl in EtOH was added dropwise at 0 °C to obtain the desired product as hydrochloride salt.

4.2.9. 2-Bromo-N,N-diethyl-2-phenylacetamide (7a)

Thionyl chloride (2.77 g, 23.3 mmol, 10.0 eq) was added dropwise to α-bromo-phenylacetic acid (**6**, 500 mg, 2.33 mmol, 1.00 eq) at 0 °C. The reaction mixture was stirred at 0 °C for 0.5 h under N_2 atmosphere and then at 78 °C for 5.5 h. After completion, the excess of thionyl chloride was distilled and reaction mixture washed with CH_2Cl_2 anhydrous (3 x 1 mL). The resulting compound 7**a** (543 mg, 2.33 mmol, 1.00 eq) was dissolved in CH_2Cl_2 anhydrous (3 mL, 766 mM), and diethylamine (289 µL, 2.79 mmol, 1.20 eq) and DIPEA (486 µL, 2.79 mmol, 1.20 eq) were added at 0 °C. The reaction mixture was stirred at rt on. After completion, the mixture was concentrated *in vacuo*, the residue dissolved in EtOAc (15 mL), washed with a saturated solution of $NaHCO_3$ (1 x 5 mL), brine (1 x 5 mL), dried (Na_2SO_4), filtered and concentrated *in vacuo*. The residue was purified by flash column chromatography (diameter of the column 2.5 cm; eluent PE/EtOAc 90:10 to 85:15). Pale yellow oil, yield 220 mg (35 %). $R_f = 0.25$ (PE/EtOAc 70:30). ^{1}H NMR (500 MHz, $CDCl_3$) δ 7.43–7.56 (m, 2H), 7.30–7.43 (m, 3H), 5.65 (s, 1H), 3.27–3.46 (m, 4H), 1.13 (td, $J = 7.3$, 18.7 Hz, 6H).

4.2.10. Ethyl 2-bromo-2-phenylacetate (7b)

The commercially available α-bromo-phenylacetic acid (**6**, 500 mg, 2.33 mmol, 1.00 eq) was dissolved in EtOH (9 mL, 240 mM). Then, H_2SO_4 (158 µL, 2.91 mmol, 1.25 eq) was added at rt. The reaction mixture was stirred at 100 °C for 5h. After completion, the reaction mixture was concentrated *in vacuo*, the residue was dissolved in EtOAc (15 mL), washed with a saturated solution of $NaHCO_3$ (1 x 5 mL), brine (1 x 5 mL), dried over Na_2SO_4, filtered and concentrated *in vacuo*. The residue was purified by flash column chromatography (diameter of the column 3 cm; eluent PE/EtOAc 100:0 to 99:1). Clear oil, yield 485 mg (85 %). $R_f = 0.25$ (PE/EtOAc 98:2). ^{1}H NMR (500 MHz, $CDCl_3$) δ 7.54–7.58 (m, 2H), 7.33–7.41 (m, 3H), 5.35 (s, 1H), 4.19–4.32 (m, 2H), 1.30 (t, $J = 7.1$ Hz, 3H).

4.2.11. tert-Butyl 4-phenethylpiperazine-1-carboxylate (9a)

The compound has been prepared using 2-phenylacetaldehyde (194 mg, 1.60 mmol, 1.00 eq) following procedure A. The residue was purified by flash column chromatography (diameter of the column 2.5 cm; eluent Hex/EtOAc 95:5 to 80:20). Yellow oil, yield 187 mg (40 %). $R_f =$

0.2 (Hex/EtOAc 95:5). ^{1}H NMR (500 MHz, $CDCl_3$ – free base) δ 7.28–7.31 (m, 1H), 7.27 (d, J = 4.9 Hz, 1H), 7.18–7.22 (m, 3H), 3.44–3.48 (m, 4H), 2.78–2.83 (m, 2H), 2.57–2.63 (m, 2H), 2.44–2.50 (m, 4H), 1.46 (s, 9H).

4.2.12. *tert-Butyl methyl(1-phenethylpiperidin-4-yl)carbamate (**9b**)*

The compound has been prepared using (2-bromoethyl)benzene (225 mg, 1.21 mmol, 1.30 eq) following procedure B. The residue was purified by flash column chromatography (diameter of the column 2.5 cm; eluent Hex/EtOAc 90:10 to 70:30). Yellow oil, yield 202 mg (68 %). R_f = 0.55 ($CHCl_3$/CH_3OH 90:10). ^{1}H NMR (200 MHz, $CDCl_3$ – free base) δ 7.12−7.36 (m, 5H), 3.08 (d, J = 11.7 Hz, 2H), 2.70–2.89 (m, 5H), 2.51–2.66 (m, 2H), 2.11 (s, 3H), 1.53–1.89 (m, 4H), 1.47 (s, 9H).

4.2.13. *tert-Butyl 4-(3-phenylpropyl)piperazine-1-carboxylate (**9c**)*

The compound has been prepared using 3-phenylpropanal (144 mg, 1.07 mmol, 1.00 eq) following procedure A. The residue was purified by flash column chromatography (diameter of the column 2.5 cm; eluent CH_2Cl_2/CH_3OH 100:0 to 90:10). Colorless oil, yield 220 mg (67 %). R_f = 0.20 (CH_2Cl_2/CH_3OH 95:5). ^{1}H NMR (500 MHz, $CDCl_3$ – free base) δ 7.25–7.32 (m, 2H), 7.15–7.21 (m, 3H), 3.39–3.48 (m, 4H), 2.64 (t, J = 7.8 Hz, 2H), 2.31–2.45 (m, 6H), 1.82 (t, J = 7.83 Hz, 2H), 1.45 (s, 9H).

4.2.14. *tert-Butyl methyl(1-(3-phenylpropyl)piperidin-4-yl)carbamate (**9d**)*

The compound has been prepared using (3-bromopropyl)benzene (181 mg, 0.91 mmol, 1.30 eq) following procedure B. The residue was purified by flash column chromatography (diameter of the column 2.5 cm; eluent Hex/EtOAc 50:50). Yellow oil, yield 140 mg (60 %). R_f = 0.55 ($CHCl_3$/CH_3OH 90:10). ^{1}H NMR (200 MHz, $CDCl_3$ – free base) δ ppm 7.11–7.35 (m, 5H), 2.97 (d, J = 11.7 Hz, 2H), 2.73 (s, 3H), 2.62 (t, J = 7.8 Hz, 2H), 2.29–2.41 (m, 2H), 1.54–2.08 (m, 9H), 1.46 (s, 9H).

4.2.15. *Ethyl 2-(4-cyclohexylpiperazin-1-yl)-2-phenylacetate (**11a, AD409**)*

The compound has been prepared using 1-cyclohexylpiperazine (**10a**, 200 mg, 1.19 mmol, 1.00 eq) following procedures C and G. The residue was purified by flash column chromatography (diameter of the column 2.5 cm; eluent CH_2Cl_2/CH_3OH 99:1). Pale yellow oil, yield 24 mg (6 %). Anal. calcd for $C_{20}H_{30}N_2O_2$: C, 72.69; H, 9.15; N, 8.48; Found: C, 72.51; H, 9.12; N, 8.41. R_f = 0.25 (CH_2Cl_2/CH_3OH 98:2). ESI-MS m/z 331.2 $[M+H]^+$. ^{1}H NMR (500 MHz, $CDCl_3$ – free base) δ 7.43 (d, J = 6.4 Hz, 2H), 7.28–7.38 (m, 3H), 4.04–4.26 (m, 2H), 3.94 (s, 1H), 2.63 (br. s., 4H), 2.48 (br. s., 4H), 2.23 (br. s., 1H), 1.87 (d, J = 8.8 Hz, 2H), 1.78 (d, J = 10.3 Hz, 2H), 1.61 (d, J = 12.2 Hz, 1H), 1.03–1.29 (m, 8H). ^{13}C NMR (126 MHz, CDCl3 – free base) δ 171.5, 135.9, 128.8, 128.5, 128.3, 74.4, 63.5, 60.9, 51.4, 48.6, 28.9, 28.8, 26.2, 25.8, 14.1.

4.2.16. *Ethyl 2-(4-(cyclohexylmethyl)piperazin-1-yl)-2-phenylacetate (**11b, AD416**)*

The compound has been prepared using 1-(cyclohexylmethyl) piperazine (**10b**, 50 mg, 0.27 mmol, 1.00 eq) following procedures C and G. The residue was purified by flash column chromatography (diameter of the column 1.5 cm; eluent Hex/EtOAc gradient 100:0 to 95:5). Pale yellow oil, yield 11 mg (12 %). Anal. calcd for $C_{21}H_{32}N_2O_2$: C, 73.22; H, 9.36; N, 8.13; Found: C, 72.95; H, 9.36; N, 8.16. R_f = 0.30 (Hex/EtOAc 95:5). ESI-MS m/z 345.2 $[M+H]^+$, 367.2 $[M+Na]^+$. ^{1}H NMR (500 MHz, $CDCl_3$ – free base) δ 7.44 (dd, J = 1.5, 7.8 Hz, 2H), 7.28–7.35 (m, 3H), 4.07–4.21 (m, 2H), 3.94 (s, 1H), 2.44 (br. s., 7H), 2.11 (d, J = 6.9 Hz, 1H), 1.61–1.77 (m, 7H), 1.44 (qd, J = 3.7, 7.1 Hz, 1H), 1.16–1.22 (m, 5H), 0.79–0.91 (m, 3H). ^{13}C NMR (126 MHz, $CDCl_3$ – free base) δ 171.7, 136.2, 129.0, 128.6, 128.4, 74.6, 65.7, 61.0, 53.5, 51.3, 35.1, 32.1, 26.9, 26.3, 14.2.

4.2.17. *Ethyl 2-(4-phenethylpiperazin-1-yl)-2-phenylacetate (**11c, AD307**)*

The compound has been prepared using **9a** (175 mg, 0.60 mmol, 1.00 eq) and **7b** (180 mg, 0.74 mmol, 1.35 eq) following procedure D. The residue was purified by flash column chromatography (diameter of the column 2.5 cm; eluent Hex/EtOAc gradient 85:15). Yellow oil, yield 85 mg (50 %). Anal. calcd for $C_{22}H_{28}N_2O_2$: C, 74.97; H, 8.01; N, 7.95; Found: C, 74.62; H, 7.99; N, 7.89. R_f = 0.30 (Hex/EtOAc 85:15). ESI-MS m/z 353.2 $[M+H]^+$, 375.1 $[M+Na]^+$. ^{1}H NMR (500 MHz, $CDCl_3$ – free base) δ 7.42−7.47 (m, 2H), 7.24−7.37 (m, 5H), 7.17−7.20 (m, 3H), 4.06−4.23 (m, 2H), 3.97 (s, 1H), 2.74−2.82 (m, 2H), 2.45−2.66 (m, 10H), 1.17−1.23 (m, 3H). ^{13}C NMR (126 MHz, $CDCl_3$ – free base) δ 171.4, 140.3, 135.9, 129.1, 128.8, 128.8, 128.7, 128.5, 128.3, 128.1, 127.1, 126.0, 125.8, 79.0, 74.5, 60.9, 60.4, 52.9, 51.1, 33.6, 14.1.

4.2.18. *Ethyl 2-phenyl-2-(4-(3-phenylpropyl)piperazin-1-yl)acetate (**11d, AD296**)*

The compound has been prepared using **9c** (220 mg, 0.72 mmol, 1.00 eq) and **7b** (169 mg, 0.70 mmol, 1.35 eq) following procedure D. The residue was purified by flash column chromatography (diameter of the column 2.5 cm; eluent Hex/EtOAc gradient from 90:10 to 70:30). Colorless oil, yield 105 mg (56 %). Anal. calcd for $C_{23}H_{30}N_2O_2$: C, 75.37; H, 8.25; N, 7.64; Found: C, 75.8; H, 8.26; N, 7.63. R_f = 0.20 (Hex/EtOAc 80:20). ESI-MS m/z 367.2 $[M+H]^+$, 389.1 $[M+Na]^+$. ^{1}H NMR (500 MHz, $CDCl_3$ – free base) δ 7.43−7.47 (m, 2H), 7.30−7.37 (m, 3H), 7.25−7.29 (m, 2H), 7.15−7.20 (m, 3H), 4.08−4.23 (m, 2H), 3.96 (s, 1H), 2.62 (t, J = 7.8 Hz, 2H), 2.41−2.59 (m, 8H), 2.35−2.41 (m, 2H), 1.78−1.83 (m, 2H), 1.18−1.23 (m, 3H). ^{13}C NMR (126 MHz, $CDCl_3$ – free base) δ 171.6, 136.0, 129.0, 128.7, 128.5, 128.4, 125.9, 74.4, 61.0, 58.0, 53.0, 51.1, 33.8, 29.8, 28.5, 14.2.

4.2.19. *Ethyl 2-((1-benzylpiperidin-4-yl)(methyl)amino)-2-phenylacetate (**12a, AD353**)*

The compound has been prepared using the commercially available 1-benzyl-*N*-methylpiperidin-4-amine (**10c**, 150 mg, 0.73 mmol, 1.00 eq) and **7b** (196 mg, 0.81 mmol, 1.10 eq) following procedure E. The residue was purified by flash column chromatography (diameter of the column 2.5 cm; eluent CH_2Cl_2/CH_3OH gradient 100:0 to 99:1). Pale yellow oil, yield 110 mg (41 %). Anal. calcd for $C_{23}H_{30}N_2O_2$: C, 75.37; H, 8.25; N, 8.64; Found: C, 75.83; H, 8.24; N, 7.68. R_f = 0.20 (CH_2Cl_2/CH_3OH 90:10). ESI-MS m/z 367.2 $[M+H]^+$, 389.1 $[M+Na]^+$. ^{1}H NMR (500 MHz, $CDCl_3$ – free base) δ 7.42–7.47 (m, 2H), 7.21–7.39 (m, 8H), 4.44 (s, 1H), 4.10–4.25 (m, 2H), 3.46 (s, 2H), 2.92 (t, J = 10.8 Hz, 2H), 2.48–2.57 (m, 1H), 2.26 (s, 3H), 1.81–1.94 (m, 2H), 1.64−1.80 (m, 4H), 1.23 (t, J = 7.1 Hz, 3H). ^{13}C NMR (126 MHz, $CDCl_3$ – free base) δ 172.6, 137.3, 129.3, 128.7, 128.5, 128.3, 128.1, 127.1, 70.3, 63.2, 60.8, 58.1, 53.5, 53.2, 33.8, 28.5, 27.4, 14.2.

4.2.20. *2-((1-Benzylpiperidin-4-yl)(methyl)amino)-N,N-diethyl-2-phenylacetamide (**12b, AD351**)*

The compound has been prepared using the commercially available 1-benzyl-*N*-methylpiperidin-4-amine (**10c**, 60.0 mg, 0.29 mmol, 1.00 eq) and **7a** (116 mg, 0.43 mmol, 1.10 eq) following procedure E. The residue was purified by flash column chromatography (diameter of the column 2.5 cm; eluent CH_2Cl_2/CH_3OH gradient 95:5). Clear oil, yield 40 mg (35 %). Anal. calcd for $C_{25}H_{35}N_3O$: C, 76.29; H, 8.96; N, 10.68; Found: C, 76.48; H, 8.98, N, 10.65. R_f = 0.50 (CH_2Cl_2/CH_3OH 90:10). ESI-MS m/z 394.2 $[M+H]^+$. ^{1}H NMR (500 MHz, $CDCl_3$ – free base) δ 7.40 (d, J = 6.9 Hz, 2H), 7.21–7.36 (m, 8H), 4.69 (s, 1H), 3.47 (s, 2H), 3.40–3.46 (m, 1H), 3.32–3.39 (m, 1H), 3.24–3.32 (m, 1H), 3.16 (s, 1H), 2.85–2.97 (m, 2H), 2.57–2.67 (m, 1H), 2.33 (s, 3H), 1.85–1.99 (m, 2H), 1.77–1.83 (m, 1H), 1.62–1.76 (m, 3H), 1.11 (t, J = 7.1 Hz, 3H), 1.00 (t, J = 7.1 Hz, 3H). ^{13}C NMR (126 MHz, $CDCl_3$ – free base) δ 171.2, 137.7, 129.2, 129.2, 128.4, 128.1, 127.6, 127.0, 66.4, 63.0, 58.2, 53.4, 53.2, 41.4, 40.3, 34.2, 29.3, 28.6, 14.2, 12.7.

4.2.21. Ethyl 2-(methyl(1-phenethylpiperidin-4-yl)amino)-2-phenylacetate (12c, AD408)

The compound has been prepared using **9b** (85.0 mg, 0.27 mmol, 1.00 eq) and **7b** (77.9 mg, 0.32 mmol, 1.20 eq) following procedure F. The residue was purified by flash column chromatography (diameter of the column 1.5 cm; eluent EtOAc/CH_3OH gradient 100:0 to 98:2). Pale yellow oil, yield 77 mg (75 %). Anal. calcd for $C_{24}H_{32}N_2O_2$: C, 75.75; H, 8.48; N, 7.36; Found: C, 75.77; H, 8.42; N, 7.35. Rf = 0.40 (EtOAc/CH_3OH 95:5). ESI-MS *m/z* 381.2 $[M+H]^+$. ^{1}H NMR (200 MHz, $CDCl_3$ – free base) δ 7.08–7.53 (m, 10H), 4.43 (s, 1H), 4.04–4.30 (m, 2H), 3.04 (d, J = 10.9 Hz, 2H), 2.71–2.86 (m, 2H), 2.44–2.62 (m, 3H), 2.26 (s, 3H), 1.60–2.06 (m, 6H), 1.22 (t, J = 7.2 Hz, 3H). ^{13}C NMR (50 MHz, $CDCl_3$ – free base) δ 172.6, 140.4, 137.3, 128.8, 128.7, 128.5, 128.5, 128.1, 126.1, 70.3, 60.8, 60.6, 58.0, 53.5, 53.3, 34.0, 33.8, 28.5, 27.3, 14.3.

4.2.22. N,N-diethyl-2-(methyl(1-phenethylpiperidin-4-yl)amino)-2-phenylacetamide (12d, AD415)

The compound has been prepared **9b** (96.0 mg, 0.30 mmol, 1.00 eq) and **7a** (97.7 mg, 0.36 mmol, 1.20 eq) following procedure F. The residue was purified by flash column chromatography (diameter of the column 2.5 cm; eluent EtOAc/CH_3OH gradient 90:10). Clear oil, yield 27 mg (22 %). Anal. calcd for $C_{26}H_{37}N_3O$: C, 76.62; H, 9.15; N, 10.31; Found: C, 76.93; H, 9.15; N, 7.31. R_f = 0.20 (EtOAc/CH_3OH 90:10). ESI-MS *m/z* 408.2 $[M+H]^+$, 430.2 $[M+Na]^+$. ^{1}H NMR (500 MHz, $CDCl_3$ – free base) δ 7.42 (d, J = 7.8 Hz, 2H), 7.34 (t, J = 7.3 Hz, 2H), 7.25–7.31 (m, 3H), 7.19 (d, J = 7.8 Hz, 3H), 4.70 (s, 1H), 3.41–3.50 (m, 1H), 3.33–3.41 (m, 1H), 3.25–3.32 (m, 1H), 3.14–3.23 (m, 1H), 3.03 (q, J = 10.0 Hz, 2H), 2.79 (t, J = 8.3 Hz, 2H), 2.64 (br. s, 1H), 2.55 (t, J = 8.3 Hz, 2H), 2.35 (s, 3H), 1.84–2.03 (m, 3H), 1.71–1.78 (m, 1H), 1.68 (q, J = 2.9 Hz, 2H), 1.12 (t, J = 7.1 Hz, 3H), 1.02 (t, J = 7.1 Hz, 3H). ^{13}C NMR (50 MHz, $CDCl_3$ – free base) δ 171.2, 140.0, 137.6, 129.2, 128.8, 128.5, 128.5, 127.8, 126.2, 66.6, 60.3, 57.7, 53.3, 53.1, 41.5, 40.4, 34.4, 33.4, 29.0, 28.2, 14.3, 12.8.

4.2.23. Ethyl 2-(methyl(1-(3-phenylpropyl)piperidin-4-yl)amino)-2-phenylacetate (12e, AD405)

The compound has been prepared using **9d** (70.5 mg, 0.21 mmol, 1.00 eq) and **7b** (61.9 mg, 0.25 mmol, 1.20 eq) following procedure F. The residue was purified by flash column chromatography (diameter of the column 1.5 cm; eluent $CHCl_3$/CH_3OH gradient 100:0 to 98:2). Pale yellow oil, yield 33 mg (40 %). Anal. calcd for $C_{25}H_{34}N_2O_2$: C, 76.1; H, 8.69; N, 7.1; Found: C, 76.2; H, 8.67; N, 7.11. R_f = 0.20 ($CHCl_3$/CH_3OH 98:2). ESI-MS *m/z* 395.2 $[M+H]^+$. ^{1}H NMR (200 MHz, $CDCl_3$ – free base) δ 6.88–7.74 (m, 10H), 4.42 (s, 1H), 4.03–4.29 (m, 2H), 2.86–3.02 (m, 2H), 2.60 (t, J = 7.6 Hz, 2H), 2.41–2.54 (m, 1H), 2.25–2.36 (m, 2H), 2.24 (s, 3H), 1.58–1.91 (m, 8H), 1.21 (t, J = 7.1 Hz, 3H). ^{13}C NMR (50 MHz, $CDCl_3$ – free base) δ 172.6, 142.3, 137.3, 128.8, 128.5, 128.5, 128.4, 128.1, 125.8, 70.3, 60.8, 58.2, 58.1, 53.6, 53.4, 33.9, 33.8, 29.0, 28.5, 27.4, 14.3.

4.2.24. N,N-Diethyl-2-(methyl(1-(3-phenylpropyl)piperidin-4-yl)amino)-2-phenylacetamide (12f, AD400)

The compound has been prepared using **9d** (71.3 mg, 0.21 mmol, 1.00 eq) and **7a** (63.0 mg, 0.23 mmol, 1.10 eq) following procedure F. The residue was purified by flash column chromatography (diameter of the column 1.5 cm; eluent EtOAc/CH_3OH gradient from 100:0 to 95:5). Clear oil, yield 10 mg (11 %). Anal. calcd for $C_{27}H_{39}N_3O$: C, 76.92; H, 9.32; N, 9.97; Found: C, 76.82; H, 9.31; N, 9.93. R_f = 0.30 (EtOAc/CH_3OH 95:5). ESI-MS *m/z* 422.3 $[M+H]^+$. ^{1}H NMR (500 MHz, $CDCl_3$ – free base) δ 7.40 (d, J = 7.3 Hz, 2H), 7.33 (t, J = 7.4 Hz, 2H), 7.24–7.31 (m, 3H), 7.14–7.22 (m, 3H), 4.69 (s, 1H), 3.40–3.49 (m, 1H), 3.32–3.40 (m, 1H), 3.24–3.31 (m, 1H), 3.13–3.22 (m, 1H), 2.95 (dd, J = 10.5, 19.8 Hz, 2H), 2.62 (t, J = 7.6 Hz, 3H), 2.32 (s, 5H), 1.90 (br. s., 1H), 1.78–1.87 (m, 4H), 1.72 (br. s, 1H), 1.65 (s, 2H), 1.11 (t, J = 7.1 Hz, 3H), 1.01 (t, J = 7.1 Hz, 3H). ^{13}C NMR (50 MHz, $CDCl_3$ – free base) δ 171.3, 142.2, 137.8, 129.3, 128.5, 128.5, 128.4, 127.8, 125.9, 66.7, 58.1, 53.6, 53.4, 41.5, 40.5, 34.3, 33.9, 29.4, 28.9, 28.6, 14.3, 12.8.

4.3. Radioligand binding assays

S1R and S2R binding affinity. Binding assays have been performed to evaluate the affinity for S1R and S2R of the developed ligands. Both assays involve the use of tris buffer (50 mM, pH 8) and liver homogenates from male Sprague Dawley rats. As regard S1R ligand binding assays, [^{3}H](+)-PTZ (2 nM; K_d = 2.9 nM) was employed as radioligand in a final volume of 0.5 mL with increasing concentrations of test compounds. Non-specific binding was measured using unlabeled PTZ (10 μM). *In vitro* S2R ligand binding assays were performed using [^{3}H] DTG (2 nM; K_d = 17.9 nM) as radioligand, PTZ (5 μM) as S1R masking agent. Unlabeled DTG (10 μM) – for the measurement of non-specific binding – and increasing concentrations of test compounds in a final volume of 0.5 mL have been used [69].

Data analysis. The K_i-values were calculated with the program GraphPad Prism® 7.0 (GraphPad Software, San Diego, CA, USA). The K_i-values are given as mean value ± SD from at least two independent experiments performed in duplicate.

4.4. Molecular modeling

Docking and post-docking analysis. The crystal structure of the human S1R bound to PD144418 (PDB ID 5HK1) and the crystal structure of the bovine S2R bound to compound Z1241145220 (PDB ID 7M95), were used for our molecular modeling studies. The receptor structures were properly processed using the same protocol reported in our previous works [12,84]. Docking simulations were carried out by means Glide v. 8.9, using the Standard Precision (SP) protocol and generating 10 poses per ligand (Glide, Schrödinger, LLC, New York, NY, 2020). Starting from the best docking pose of **12a** and **12c**, a post-docking energy minimization was performed by using the eMBrAcE tool, implemented in the Schrödinger suite (MacroModel v13.0) and the binding energies (E) of the receptor-ligand complexes were calculated (MacroModel; Schrödinger, LLC, New York, NY, USA, 2020) [63].

Ligand preparation. All the compounds were prepared by means of LigPrep tool. Hydrogens were added, salts were removed, and ionization states were calculated using Epik at pH 7.4 and OPLS_2005 as force field (LigPrep, Schrödinger, LLC, New York, NY, 2020).

4.5. In vitro toxicity

Cell Cultures. Human microglia HMC3 (ATCC® CRL-3304) and human skin fibroblasts WS1 (ATCC® CRL-1502™) were purchased from the American Type Culture Collection (ATCC®; Manassas, VA, USA) and cultured in EMEM medium, containing 10 % fetal bovine serum (FBS), 2 mM L-glutamine, 100 units/mL penicillin and 100 μg/mL streptomycin. All media and reagents were from Euroclone S.p.A. (Pero, Milan, Italy).

Cell Proliferation and Cytotoxicity. For cell proliferation, HMC3 or WS1 cells (3×10^3) were seeded in 96-well plates and grown at optimum culture conditions for 72h (at a confluence of ~60 %). Then, cells were treated with the indicated compounds for an additional 48h. In contrast, cytotoxicity was assessed in confluent WS1 cell monolayers, treated for 24h with the indicated chemicals. For all these assays, at the end of treatments cells were fixed (in 4 % paraformaldehyde) and stained with acridine orange solution (50 μg/mL), as previously described [64]. Acridine orange staining was then evaluated by measuring the fluorescence (excitation 485/20 nm, emission 528/20 nm) with a microplate reader (Synergy HT, BioTek).

Statistical Analysis. Results are shown as mean ± SEM of three independent experiments performed in triplicate. Statistical comparisons were performed by ANOVA one-way. P values were considered significant at $\alpha \leq 0.05$. All analyses were done with GraphPad Prism 9.3.1 (GraphPad Software, Inc., San Diego, CA).

4.6. In vivo

Experimental Animals. Experiments were performed in wild-type (WT) female CD-1 mice (Charles River, Barcelona, Spain) and in S1R knockout (KO) mice (Animal Experimentation Unit - CIC UGR, Granada, Spain), weighing 25–30 g (8–11 weeks old). Animals were housed in colony cages (10 mice per cage), in a temperature-controlled room (22 ± 2 °C) with an automatic 12-h light/dark cycle (08:00–20:00 h). An igloo and a plastic tunnel were placed in each housing cage for environmental enrichment. Animals were fed a standard laboratory diet and tap water ad libitum until the beginning of the experiments. The behavioral experiments were performed during the light phase (from 9:00 a.m. to 3:00 p.m.). The mice were randomized to treatment groups, testing each day a balanced number of animals from several experimental groups, and they were also tested randomly throughout the estrous cycle. Mice were handled in accordance with international standards (European Communities Council directive 2010/63), and the experimental protocols were approved by regional (Junta de Andalucía) and Institutional (Research Ethics Committee of the University of Granada) authorities.

Drugs and Drug Administration. The experimental compounds were dissolved in 1 % Tween-80 (Merck KGaA, Darmstadt, Germany) in physiological sterile saline (0.9 % NaCl). As S1R control drugs, we used the S1R antagonist S1RA (E−52862.HCl; 4-[2-[[5-methyl-1-(2-naphthalenyl)-1H-pyrazol-3-yl]oxy]ethyl] morpholine) and the S1R agonist PRE-084 (2-(4-morpholinethyl)1]-phenyl cyclohexane carboxylate hydrochloride) (both DC Chemicals, Shanghai, China) [68]. Drug solutions were prepared immediately before the start of the experiments and injected s.c. in a volume of 5 mL/kg into the interscapular area. S1RA or the experimental drugs tested were injected 45 min before the behavioral evaluation. To evaluate the sensitivity of drug effects to S1R agonism, we s.c. administered PRE-084 5 min before the drugs tested.

Capsaicin (Sigma-Aldrich, Madrid, Spain) was dissolved in 1 % DMSO in physiological sterile saline to a concentration of 1 μg/20 μL [64], and injected intraplantarly (i.pl.) into the right hindpaw, 15 min before the behavioral test. PGE2 (Tocris Cookson Ltd., Bristol, UK) was dissolved in sterile physiological saline (0.9 % NaCl) to a concentration of 0.5 nmol/20 μL [70] and injected i.pl. into the right hindpaw, 10 min before the behavioral test. Both algogenic chemicals were injected in a volume of 20 μL using a 1710 TLL Hamilton microsyringe (Teknokroma, Barcelona, Spain) with a 301/2-gauge needle, and control animals were injected with the same volume of the vehicle of capsaicin or PGE2.

Evaluation of Capsaicin-Induced Secondary Mechanical Hypersensitivity. Animals were placed for 2h in individual black-walled test compartments, which were situated on an elevated mesh-bottom platform with a 0.5 cm^2 grid to provide access to the ventral surface of the hind paws. Punctate mechanical stimulation was applied with a Dynamic Plantar Aesthesiometer (Ugo Basile, Varese, Italy) 15 min after the administration of capsaicin or its vehicle (i.e., 45 min after drug injection). Briefly, a nonflexible filament (0.5 mm diameter) was electronically driven into the ventral side of the right hind paw at least 5 mm away from the site of the injection toward the fingers. The intensity of the stimulation was set at 0.5g force [66]. When a paw withdrawal response occurred, the stimulus was automatically terminated, and the response latency was recorded. The filament was applied three times, separated by intervals of 0.5 min. The mean value of the three trials was considered the withdrawal latency time of the animal. A cutoff time of 50 s was used in each trial.

Assessment of Mechanical Hyperalgesia. The animals were placed in the experimental room for a 1h acclimation period before starting the experiments. Mechanical hypersensitivity was assessed with the paw pressure test following a previously described protocol [70]. Blunt mechanical stimulation was applied to the right hindpaw with an Analgesimeter (Model 37215, Ugo-Basile, Varese, Italy) 10 min after the administration of PGE2 or its vehicle (i.e., 45 min after drug injection). Briefly, the mice were gently pincer grasped between the thumb and index fingers by the skin above the interscapular area. A blunt cone-shaped paw-presser was applied at a constant intensity of 100 g to the dorsal surface of the hindpaw until the animal showed a struggle response. The struggle latency was measured with a chronometer. The test was done three times with a 1-min interval between stimulations, and the mean value of the three trials was recorded as the animal's struggle latency.

4.7. Preliminary ADMET profile

Chemical Stability. Evaluation of chemical stability for compound **12a** has been performed in 50 mM Phosphate Buffer (pH 7.4) as previously reported [69]. The solution was incubated at 37 ± 0.5 °C, and at regular intervals, an amount of the reaction mixture was withdrawn and added of ACN. Three individual experiments were run in triplicate. The half-life ($t_{1/2}$) of compound **12a** was determined by fitting the data with one phase exponential decay equation using GraphPad Prism 9.0 (San Diego, CA, USA).

Water Solubility. Aqueous solubility was determined by UHPLC-PDA analysis [69]. An amount of 5 mg of **12a** as free base, was weighed and added to 1 mL of ultrapure water. The suspension was shaken at rt for 24h and then centrifuged. The supernatant was filtered and diluted in MeOH before analysis. The compound is quantified against a methanol calibration curve built over 7 dilution concentrations.

Measure of hERG Activity. Electrophysiological experiments were performed in CHO e K1 cells that express human ERG using a Qube APC assay. Compound **12a** has been tested employing 6 different concentrations ranging from 10^{-10} to 10^{-5} M using serial dilution by Eurofins Panlabs (St Charles, MO, United States) according to their standard assay protocol.

Measurement of logP and logD. Lipophilicity of compound **12a** was measured between *n*-octanol and water using a previously published protocol [85,86]. Haloperidol has been used as reference compound. For the preparation of the solutions for the calibration curves, a convenient mass of compound was dissolved in DMSO in order to obtain a 10 mM stock solution. Different concentrations (5 μM, 10 μM, 25 μM, 50 μM, 75 μM, 100 μM and 150 μM) have been prepared by diluting the stock solution in *n*-octanol, distilled water or PBS. The UV absorption spectra were recorded with a Hitachi U-2900 spectrophotometer, using quartz cells of 1 cm optic path length.

In order to determine the logP value, a mixture of *n*-octanol and water (1:1, v/v) was prepared and stirred overnight to ensure mutual saturation of both phases. An opportune amount of the sample was accurately weighed and dissolved in a sufficient volume of *n*-octanol saturated with water to achieve a final concentration of 10 mM. Subsequently, the same volume of water saturated with *n*-octanol was added and the biphasic mixture was stirred for 2h at rt to allow for the partitioning between the two phases. After stirring, the phases were allowed to separate overnight using a separating funnel. As a blank for absorbance measurements was used a similar mixture in each case but changing *n*-octanol in place of the sample stock solution. An aliquot of 1 mL was taken from each phase, filtered through 0.45 μm LLG syringe filters, and centrifuged at 15,000 rpm for 15 min. The samples were then analyzed using UV–Vis spectrophotometry. The concentration of **12a** and haloperidol in the *n*-octanol phase was obtained by interpolation of the absorbance measured on the calibration curve.

LogD[pH 7.4] measurements have been conducted in a similar manner, by using a mixture (1:1, v/v) of *n*-octanol and PBS (pH = 7.4) left to stir overnight to ensure mutual saturation of both phases [87].

CRediT authorship contribution statement

Giuseppe Cosentino: Writing – review & editing, Writing – original draft, Investigation. **Maria Dichiara:** Writing – review & editing, Writing – original draft, Supervision, Methodology, Investigation, Data curation, Conceptualization. **Francesca Alessandra Ambrosio:** Writing

– original draft, Investigation. **Claudia Giovanna Leotta:** Investigation. **Giosuè Costa:** Writing – original draft, Investigation. **Francesca Procopio:** Writing – original draft, Investigation. **Giuliana Costanzo:** Investigation. **Alessandro Raffa:** Investigation. **Antonia Artacho-Cordón:** Investigation. **M. Carmen Ruiz-Cantero:** Investigation. **Lorella Pasquinucci:** Writing – review & editing, Supervision. **Agostino Marrazzo:** Writing – review & editing, Supervision, Funding acquisition. **Giovanni Mario Pitari:** Writing – original draft, Supervision, Methodology. **Enrique J. Cobos:** Writing – original draft, Supervision, Methodology, Funding acquisition, Data curation. **Stefano Alcaro:** Writing – original draft, Supervision, Methodology, Data curation. **Emanuele Amata:** Writing – review & editing, Writing – original draft, Supervision, Methodology, Funding acquisition, Data curation, Conceptualization.

Declaration of competing interest

The authors declare that they have no known competing financial interests or personal relationships that could have appeared to influence the work reported in this paper.

Acknowledgments

This research was funded by Italian Minister of University and Research projects PRIN 2017−201744BN5T and PRIN 2022−P20224L3NK; European Cooperation in Science and Technology (COST) CA23156 - European Network for Sigma-1 Receptor as a Therapeutic Opportunity. This study was partially supported by the Spanish State Research Agency (10.13039/501100011033) under the auspices of the Spanish Ministry of Science, Innovation and Universities (grant number PID2019-108691RB-I00), the Andalusian Regional Government (grant CTS-109), and the Unit of Excellence 'UNETE' from the University of Granada (reference UCE-PP2017-05).

Appendix A. Supplementary data

Supplementary data to this article can be found online at https://doi.org/10.1016/j.ejmech.2024.117037.

Data availability

Data will be made available on request.

References

[1] N.B. Finnerup, R. Kuner, T.S. Jensen, Neuropathic pain: from mechanisms to treatment, Physiol. Rev. 101 (2021) 259–301.
[2] F. Petzke, T. Tölle, M.A. Fitzcharles, W. Häuser, Cannabis-based Medicines and medical cannabis for chronic neuropathic pain, CNS Drugs 36 (2022) 31–44.
[3] E. Balzani, A. Fanelli, V. Malafoglia, M. Tenti, S. Ilari, A. Corraro, C. Muscoli, W. Raffaeli, A review of the clinical and therapeutic implications of neuropathic pain, Biomedicines 9 (2021).
[4] A. Szczudlik, J. Dobrogowski, J. Wordliczek, A. Stępień, M. Krajnik, W. Leppert, J. Woroń, A. Przeklasa-Muszyńska, M. Kocot-Kępska, R. Zajączkowska, M. Janecki, A. Adamczyk, M. Malec-Milewska, Diagnosis and management of neuropathic pain: review of literature and recommendations of the Polish Association for the study of pain and the Polish Neurological Society - part one, Neurol. Neurochir. Pol. 48 (2014) 262–271.
[5] K.M. Foley, Opioids and chronic neuropathic pain, N. Engl. J. Med. 348 (2003) 1279–1281.
[6] A. Mu, E. Weinberg, D.E. Moulin, H. Clarke, Pharmacologic management of chronic neuropathic pain: review of the Canadian Pain Society consensus statement, Canadian family physician Medecin de famille canadien 63 (2017) 844–852.
[7] G.W. Zamponi, J. Striessnig, A. Koschak, A.C. Dolphin, The physiology, pathology, and pharmacology of voltage-gated calcium channels and their future therapeutic potential, Pharmacol. Rev. 67 (2015) 821–870.
[8] J. Pergolizzi Jr., G. Varrassi, The emerging role of sigma receptors in pain medicine, Cureus 15 (2023) e42626.
[9] S.M. Wang, N. Goguadze, Y. Kimura, Y. Yasui, B. Pan, T.Y. Wang, Y. Nakamura, Y. T. Lin, Q.H. Hogan, K.L. Wilson, T.P. Su, H.E. Wu, Genomic action of sigma-1 receptor chaperone relates to neuropathic pain, Mol. Neurobiol. 58 (2021) 2523–2541.
[10] M.P. Davis, Sigma-1 receptors and animal studies centered on pain and analgesia, Expet Opin. Drug Discov. 10 (2015) 885–900.
[11] P. Sánchez-Blázquez, A. Pozo-Rodrigálvarez, M. Merlos, J. Garzón, The sigma-1 receptor antagonist, S1RA, reduces stroke damage, ameliorates post-stroke neurological deficits and suppresses the overexpression of MMP-9, Mol. Neurobiol. 55 (2018) 4940–4951.
[12] M. Dichiara, F.A. Ambrosio, S.M. Lee, M.C. Ruiz-Cantero, J. Lombino, A. Coricello, G. Costa, D. Shah, G. Costanzo, L. Pasquinucci, K.N. Son, G. Cosentino, R. González-Cano, A. Marrazzo, V.K. Aakalu, E.J. Cobos, S. Alcaro, E. Amata, Discovery of AD258 as a sigma receptor ligand with potent antiallodynic activity, J. Med. Chem. 66 (2023) 11447–11463.
[13] G. Gris, E. Portillo-Salido, B. Aubel, Y. Darbaky, K. Deseure, J.M. Vela, M. Merlos, D. Zamanillo, The selective sigma-1 receptor antagonist E-52862 attenuates neuropathic pain of different aetiology in rats, Sci. Rep. 6 (2016) 24591.
[14] M. Merlos, L. Romero, D. Zamanillo, C. Plata-Salamán, J.M. Vela, Sigma-1 receptor and pain, handbook of experimental, pharmacology 244 (2017) 131–161.
[15] A. Piechal, A. Jakimiuk, D. Mirowska-Guzel, Sigma receptors and neurological disorders, Pharmacol. Rep. : PR 73 (2021) 1582–1594.
[16] J.A. Fishback, M.J. Robson, Y.T. Xu, R.R. Matsumoto, Sigma receptors: potential targets for a new class of antidepressant drug, Pharmacol. Therapeut. 127 (2010) 271–282.
[17] T.Y. Weng, S.A. Tsai, T.P. Su, Roles of sigma-1 receptors on mitochondrial functions relevant to neurodegenerative diseases, J. Biomed. Sci. 24 (2017) 74.
[18] M.V. Voronin, Y.V. Vakhitova, S.B. Seredenin, Chaperone Sigma1R and antidepressant effect, Int. J. Mol. Sci. 21 (2020).
[19] S. Castany, X. Codony, D. Zamanillo, M. Merlos, E. Verdú, P. Boadas-Vaello, Repeated sigma-1 receptor antagonist MR309 administration modulates central neuropathic pain development after spinal cord injury in mice, Front. Pharmacol. 10 (2019) 222.
[20] D. Zamanillo, L. Romero, M. Merlos, J.M. Vela, Sigma 1 receptor: a new therapeutic target for pain, Eur. J. Pharmacol. 716 (2013) 78–93.
[21] L. Zvejniece, E. Vavers, B. Svalbe, R. Vilskersts, I. Domracheva, M. Vorona, G. Veinberg, I. Misane, I. Stonans, I. Kalvinsh, M. Dambrova, The cognition-enhancing activity of E1R, a novel positive allosteric modulator of sigma-1 receptors, Br. J. Pharmacol. 171 (2014) 761–771.
[22] H. Wei, Z. Chen, A. Koivisto, A. Pertovaara, Spinal mechanisms contributing to the development of pain hypersensitivity induced by sphingolipids in the rat, Pharmacol. Rep. : PR 73 (2021) 672–679.
[23] S. Couly, N. Goguadze, Y. Yasui, Y. Kimura, S.M. Wang, N. Sharikadze, H.E. Wu, T. P. Su, Knocking out sigma-1 receptors reveals diverse health problems, Cell. Mol. Neurobiol. 42 (2022) 597–620.
[24] S. Castany, G. Gris, J.M. Vela, E. Verdú, P. Boadas-Vaello, Critical role of sigma-1 receptors in central neuropathic pain-related behaviours after mild spinal cord injury in mice, Sci. Rep. 8 (2018) 3873.
[25] K.N. Gurba, R. Chaudhry, S. Haroutounian, Central neuropathic pain syndromes: current and emerging pharmacological strategies, CNS Drugs 36 (2022) 483–516.
[26] K. Kohno, R. Shirasaka, K. Yoshihara, S. Mikuriya, K. Tanaka, K. Takanami, K. Inoue, H. Sakamoto, Y. Ohkawa, T. Masuda, M. Tsuda, A spinal microglia population involved in remitting and relapsing neuropathic pain, Science (New York, N.Y.) 376 (2022) 86–90.
[27] G. Chen, Y.Q. Zhang, Y.J. Qadri, C.N. Serhan, R.R. Ji, Microglia in pain: detrimental and protective roles in pathogenesis and resolution of pain, Neuron 100 (2018) 1292–1311.
[28] K. Inoue, M. Tsuda, Microglia in neuropathic pain: cellular and molecular mechanisms and therapeutic potential, Nat. Rev. Neurosci. 19 (2018) 138–152.
[29] M.H. Yi, Y.U. Liu, K. Liu, T. Chen, D.B. Bosco, J. Zheng, M. Xie, L. Zhou, W. Qu, L. J. Wu, Chemogenetic manipulation of microglia inhibits neuroinflammation and neuropathic pain in mice, Brain Behav. Immun. 92 (2021) 78–89.
[30] L. Nguyen, N. Kaushal, M.J. Robson, R.R. Matsumoto, Sigma receptors as potential therapeutic targets for neuroprotection, Eur. J. Pharmacol. 743 (2014) 42–47.
[31] P. Linciano, C. Sorbi, G. Rossino, D. Rossi, A. Marsala, N. Denora, M. Bedeschi, N. Marino, G. Miserocchi, G. Dondio, M. Peviani, A. Tesei, S. Collina, S. Franchini, Novel S1R agonists counteracting NMDA excitotoxicity and oxidative stress: a step forward in the discovery of neuroprotective agents, Eur. J. Med. Chem. 249 (2023).
[32] L. Nguyen, B.P. Lucke-Wold, S.A. Mookerjee, J.Z. Cavendish, M.J. Robson, A. L. Scandinaro, R.R. Matsumoto, Role of sigma-1 receptors in neurodegenerative diseases, J. Pharmacol. Sci. 127 (2015) 17–29.
[33] J. Cuevas, A. Rodriguez, A. Behensky, C. Katnik, Afobazole modulates microglial function via activation of both sigma-1 and sigma-2 receptors, J. Pharmacol. Exp. Therapeut. 339 (2011) 161–172.
[34] B. Bourrié, E. Bribes, N. De Nys, M. Esclangon, L. Garcia, S. Galiègue, P. Lair, R. Paul, C. Thomas, J.C. Vernières, P. Casellas, SSR125329A, a high affinity sigma receptor ligand with potent anti-inflammatory properties, Eur. J. Pharmacol. 456 (2002) 123–131.
[35] J. Zhao, Y. Ha, G.I. Liou, G.B. Gonsalvez, S.B. Smith, K.E. Bollinger, Sigma receptor ligand, (+)-pentazocine, suppresses inflammatory responses of retinal microglia, Investigative ophthalmology & visual science 55 (2014) 3375–3384.
[36] L. Guo, T. Gao, X. Jia, C. Gao, H. Tian, Y. Wei, W. Lu, Z. Liu, Y. Wang, SKF83959 attenuates memory impairment and depressive-like behavior during the latent period of epilepsy via allosteric activation of the sigma-1 receptor, ACS Chem. Neurosci. 13 (2022) 3198–3209.
[37] M.J. Robson, R.C. Turner, Z.J. Naser, C.R. McCurdy, J.D. Huber, R.R. Matsumoto, SN79, a sigma receptor ligand, blocks methamphetamine-induced microglial activation and cytokine upregulation, Exp. Neurol. 247 (2013) 134–142.

[38] A.A. Hall, Y. Herrera, C.T. Ajmo Jr., J. Cuevas, K.R. Pennypacker, Sigma receptors suppress multiple aspects of microglial activation, Glia 57 (2009) 744–754.
[39] B.N. Lizama, J. Kahle, S.M. Catalano, A.O. Caggiano, M. Grundman, M.E. Hamby, Sigma-2 receptors-from basic biology to therapeutic target: a focus on age-related degenerative diseases, Int. J. Mol. Sci. (2023) 24.
[40] M.S. Yousuf, J.J. Sahn, H. Yang, E.T. David, S. Shiers, M. Mancilla Moreno, J. Iketem, D.M. Royer, C.D. Garcia, J. Zhang, V.M. Hong, S.M. Mian, A. Ahmad, B. J. Kolber, D.J. Liebl, S.F. Martin, T.J. Price, Highly specific σ(2)R/TMEM97 ligand FEM-1689 alleviates neuropathic pain and inhibits the integrated stress response, Proceedings of the National Academy of Sciences of the United States of America 120 (2023) e2306090120.
[41] J.J. Sahn, G.L. Mejia, P.R. Ray, S.F. Martin, T.J. Price, Sigma 2 receptor/tmem97 agonists produce long lasting antineuropathic pain effects in mice, ACS Chem. Neurosci. 8 (2017) 1801–1811.
[42] L.L. Wilson, A.R. Alleyne, S.O. Eans, T.J. Cirino, H.M. Stacy, M. Mottinelli, S. Intagliata, C.R. McCurdy, J.P. McLaughlin, Characterization of CM-398, a novel selective sigma-2 receptor ligand, as a potential therapeutic for neuropathic pain, Molecules (2022) 27.
[43] B. Yi, J.J. Sahn, P.M. Ardestani, A.K. Evans, L.L. Scott, J.Z. Chan, S. Iyer, A. Crisp, G. Zuniga, J.T. Pierce, S.F. Martin, M. Shamloo, Small molecule modulator of sigma 2 receptor is neuroprotective and reduces cognitive deficits and neuroinflammation in experimental models of Alzheimer's disease, J. Neurochem. 140 (2017) 561–575.
[44] N. Ye, W. Qin, S. Tian, Q. Xu, E.A. Wold, J. Zhou, X.C. Zhen, Small molecules selectively targeting sigma-1 receptor for the treatment of neurological diseases, J. Med. Chem. 63 (2020) 15187–15217.
[45] A.N. Fallica, V. Ciaffaglione, M.N. Modica, V. Pittalà, L. Salerno, E. Amata, A. Marrazzo, G. Romeo, S. Intagliata, Structure-activity relationships of mixed σ1R/σ2R ligands with antiproliferative and anticancer effects, Bioorg. Med. Chem. 73 (2022).
[46] M. Burns, N. Guadagnoli, C.R. McCurdy, Advances with the discovery and development of novel sigma 1 receptor antagonists for the management of pain, Expet Opin. Drug Discov. 18 (2023) 693–705.
[47] B. Álvarez-Pérez, A. Bagó-Mas, M. Deulofeu, J.M. Vela, M. Merlos, E. Verdú, P. Boadas-Vaello, Long-lasting nociplastic pain modulation by repeated administration of sigma-1 receptor antagonist BD1063 in fibromyalgia-like mouse models, Int. J. Mol. Sci. 23 (2022).
[48] S. Riganas, I. Papanastasiou, G.B. Foscolos, A. Tsotinis, G. Serin, J.F. Mirjolet, K. Dimas, V.N. Kourafalos, A. Eleutheriades, V.I. Moutsos, H. Khan, S. Georgakopoulou, A. Zaniou, M. Prassa, M. Theodoropoulou, A. Mantelas, S. Pondiki, A. Vamvakides, New adamantane phenylalkylamines with σ-receptor binding affinity and anticancer activity, associated with putative antagonism of neuropathic pain, J. Med. Chem. 55 (2012) 10241–10261.
[49] M. Déciga-Campos, L.A. Melo-Hernández, H. Torres-Gómez, B. Wünsch, D. Schepmann, M.E. González-Trujano, J. Espinosa-Juárez, F.J. López-Muñoz, G. Navarrete-Vázquez, Design and synthesis of N-(benzylpiperidinyl)-4-fluorobenzamide: a haloperidol analog that reduces neuropathic nociception via σ(1) receptor antagonism, Life Sci. 245 (2020) 117348.
[50] R. Ventura-Martínez, G.E. Ángeles-López, D. González-Ugalde, T. Domínguez-Páez, G. Navarrete-Vázquez, R. Jaimez, M. Déciga-Campos, Antinociceptive effect of LMH-2, a new sigma-1 receptor antagonist analog of haloperidol, on the neuropathic pain of diabetic mice, Biomedicine & pharmacotherapy = Biomedecine & pharmacotherapie 174 (2024) 116524.
[51] T. Niitsu, M. Iyo, K. Hashimoto, Sigma-1 receptor agonists as therapeutic drugs for cognitive impairment in neuropsychiatric diseases, Curr. Pharmaceut. Des. 18 (2012) 875–883.
[52] R. Urfer, H.J. Moebius, D. Skoloudik, E. Santamarina, W. Sato, S. Mita, K.W. Muir, Phase II trial of the Sigma-1 receptor agonist cutamesine (SA4503) for recovery enhancement after acute ischemic stroke, Stroke 45 (2014) 3304–3310.
[53] K. Sałaciak, K. Pytka, Revisiting the sigma-1 receptor as a biological target to treat affective and cognitive disorders, Neurosci. Biobehav. Rev. 132 (2022) 1114–1136.
[54] T. Maurice, Protection by sigma-1 receptor agonists is synergic with donepezil, but not with memantine, in a mouse model of amyloid-induced memory impairments, Behav. Brain Res. 296 (2016) 270–278.
[55] M. Page, N. Pacico, S. Ourtioualous, T. Deprez, K. Koshibu, Procognitive compounds promote neurite outgrowth, Pharmacology 96 (2015) 131–136.
[56] T.R. Anderson, R.D. Andrew, Spreading depression: imaging and blockade in the rat neocortical brain slice, Journal of neurophysiology 88 (2002) 2713–2725.
[57] L. De Luca, L. Lombardo, S. Mirabile, A. Marrazzo, M. Dichiara, G. Cosentino, E. Amata, R. Gitto, Discovery and computational studies of piperidine/piperazine-based compounds endowed with sigma receptor affinity, RSC Med. Chem. 14 (2023) 1734–1742.
[58] K. Szczepańska, S. Podlewska, M. Dichiara, D. Gentile, V. Patamia, N. Rosier, D. Mönnich, M.C. Ruiz Cantero, T. Karcz, D. Łażewska, A. Siwek, S. Pockes, E. J. Cobos, A. Marrazzo, H. Stark, A. Rescifina, A.J. Bojarski, E. Amata, K. Kieć-Kononowicz, Structural and molecular insight into piperazine and piperidine derivatives as histamine H(3) and sigma-1 receptor antagonists with promising antinociceptive properties, ACS Chem. Neurosci. 13 (2022) 1–15.
[59] X. Guitart, X. Codony, X. Monroy, Sigma receptors: biology and therapeutic potential, Psychopharmacology 174 (2004) 301–319.
[60] T. Maurice, T.P. Su, The pharmacology of sigma-1 receptors, Pharmacol. Therapeut. 124 (2009) 195–206.
[61] H.R. Schmidt, S. Zheng, E. Gurpinar, A. Koehl, A. Manglik, A.C. Kruse, Crystal structure of the human σ1 receptor, Nature 532 (2016) 527–530.
[62] R.A. Glennon, Pharmacophore identification for sigma-1 (sigma1) receptor binding: application of the "deconstruction-reconstruction-elaboration" approach, Mini reviews in medicinal chemistry 5 (2005) 927–940.
[63] F. Mohamadi, N.G.J. Richards, W.C. Guida, R. Liskamp, M. Lipton, C. Caufield, G. Chang, T. Hendrickson, W.C. Still, Macromodel—an integrated software system for modeling organic and bioorganic molecules using molecular mechanics, J. Comput. Chem. 11 (1990) 440–467.
[64] W.E. Hathaway, L.A. Newby, J.H. Githens, The acridine orange viability test applied to bone marrow cells. II. Correlation with an in vivo irradiated mouse assay, Cryobiology 2 (1965) 143–146.
[65] C.J. Woolf, Central sensitization: implications for the diagnosis and treatment of pain, Pain 152 (2011) S2–s15.
[66] J.M. Entrena, E.J. Cobos, F.R. Nieto, C.M. Cendán, G. Gris, E. Del Pozo, D. Zamanillo, J.M. Baeyens, Sigma-1 receptors are essential for capsaicin-induced mechanical hypersensitivity: studies with selective sigma-1 ligands and sigma-1 knockout mice, Pain 143 (2009) 252–261.
[67] H. Gottrup, G. Juhl, A.D. Kristensen, R. Lai, B.A. Chizh, J. Brown, F.W. Bach, T. S. Jensen, Chronic oral gabapentin reduces elements of central sensitization in human experimental hyperalgesia, Anesthesiology 101 (2004) 1400–1408.
[68] J.L. Díaz, M. García, A. Torrens, A.M. Caamaño, J. Enjo, C. Sicre, A. Lorente, A. Port, A. Montero, S. Yeste, I. Álvarez, M. Martín, R. Maldonado, B. de la Puente, A. Vidal-Torres, C.M. Cendán, J.M. Vela, C. Almansa, EST64454: a highly soluble σ(1) receptor antagonist clinical candidate for pain management, J. Med. Chem. 63 (2020) 14979–14988.
[69] M. Dichiara, A. Artacho-Cordón, R. Turnaturi, M. Santos-Caballero, R. González-Cano, L. Pasquinucci, C. Barbaraci, I. Rodríguez-Gómez, M. Gómez-Guzmán, A. Marrazzo, E.J. Cobos, E. Amata, Dual Sigma-1 receptor antagonists and hydrogen sulfide-releasing compounds for pain treatment: design, synthesis, and pharmacological evaluation, Eur. J. Med. Chem. 230 (2022) 114091.
[70] M.C. Ruiz-Cantero, E. Cortés-Montero, A. Jain, Á. Montilla-García, I. Bravo-Caparrós, J. Shim, P. Sánchez-Blázquez, C.J. Woolf, J.M. Baeyens, E.J. Cobos, The sigma-1 receptor curtails endogenous opioid analgesia during sensitization of TRPV1 nociceptors, Br. J. Pharmacol. 180 (2023) 1148–1167.
[71] M.C. Ruiz-Cantero, M. Huerta, M. Tejada, M. Santos-Caballero, E. Fernández-Segura, F.J. Cañizares, J.M. Entrena, J.M. Baeyens, E.J. Cobos, Sigma-1 receptor agonism exacerbates immune-driven nociception: role of TRPV1 + nociceptors, Biomedicine & pharmacotherapy = Biomedecine & pharmacotherapie 167 (2023) 115534.
[72] M.A. Tejada, A. Montilla-García, C. Sánchez-Fernández, J.M. Entrena, G. Perazzoli, J.M. Baeyens, E.J. Cobos, Sigma-1 receptor inhibition reverses acute inflammatory hyperalgesia in mice: role of peripheral sigma-1 receptors, Psychopharmacology 231 (2014) 3855–3869.
[73] I. Bravo-Caparrós, G. Perazzoli, S. Yeste, D. Cikes, J.M. Baeyens, E.J. Cobos, F. R. Nieto, Sigma-1 receptor inhibition reduces neuropathic pain induced by partial sciatic nerve transection in mice by opioid-dependent and -independent mechanisms, Front. Pharmacol. 10 (2019) 613.
[74] A. Sharma, M. Sharma, S.B. Bharate, N-benzyl piperidine fragment in drug discovery, ChemMedChem 19 (2024) e202400384.
[75] J.V. Singh, S. Thakur, N. Kumar, H. Singh, V.S. Mithu, H. Singh, K. Bhagat, H. K. Gulati, A. Sharma, H. Singh, S. Sharma, P.M.S. Bedi, Donepezil-inspired multitargeting indanone derivatives as effective anti-alzheimer's agents, ACS Chem. Neurosci. 13 (2022) 733–750.
[76] L. Brunetti, R. Leuci, A. Carrieri, M. Catto, S. Occhineri, G. Vinci, L. Gambacorta, H. Baltrukevich, S. Chaves, A. Laghezza, C.D. Altomare, P. Tortorella, M.A. Santos, F. Loiodice, L. Piemontese, Structure-based design of novel donepezil-like hybrids for a multi-target approach to the therapy of Alzheimer's disease, Eur. J. Med. Chem. 237 (2022) 114358.
[77] M.J. Caterina, M.A. Schumacher, M. Tominaga, T.A. Rosen, J.D. Levine, D. Julius, The capsaicin receptor: a heat-activated ion channel in the pain pathway, Nature 389 (1997) 816–824.
[78] N. El Tayar, H. Van de Waterbeemd, B. Testa, Lipophilicity measurements of protonated basic compounds by reversed-phase high-performance liquid chromatography: II. Procedure for the determination of a lipophilic index measured by reversed-phase high-performance liquid chromatography, J. Chromatogr. A 320 (1985) 305–312.
[79] M. Dichiara, B. Amata, R. Turnaturi, A. Marrazzo, E. Amata, Tuning properties for blood-brain barrier permeation: a statistics-based analysis, ACS Chem. Neurosci. 11 (2020) 34–44.
[80] J.L. Díaz, U. Christmann, A. Fernández, A. Torrens, A. Port, R. Pascual, I. Álvarez, J. Burgueño, X. Monroy, A. Montero, A. Balada, J.M. Vela, C. Almansa, Synthesis and structure-activity relationship study of a new series of selective σ(1) receptor ligands for the treatment of pain: 4-aminotriazoles, J. Med. Chem. 58 (2015) 2441–2451.
[81] J.L. Díaz, R. Cuberes, J. Berrocal, M. Contijoch, U. Christmann, A. Fernández, A. Port, J. Holenz, H. Buschmann, C. Laggner, M.T. Serafini, J. Burgueño, D. Zamanillo, M. Merlos, J.M. Vela, C. Almansa, Synthesis and biological evaluation of the 1-arylpyrazole class of σ(1) receptor antagonists: identification of 4-{2-[5-methyl-1-(naphthalen-2-yl)-1H-pyrazol-3-yloxy]ethyl}morpholine (S1RA, E-52862), J. Med. Chem. 55 (2012) 8211–8224.
[82] A. Garrido, A. Lepailleur, S.M. Mignani, P. Dallemagne, C. Rochais, hERG toxicity assessment: useful guidelines for drug design, Eur. J. Med. Chem. 195 (2020) 112290.
[83] W.S. Redfern, L. Carlsson, A.S. Davis, W.G. Lynch, I. MacKenzie, S. Palethorpe, P. K. Siegl, I. Strang, A.T. Sullivan, R. Wallis, A.J. Camm, T.G. Hammond, Relationships between preclinical cardiac electrophysiology, clinical QT interval

prolongation and torsade de pointes for a broad range of drugs: evidence for a provisional safety margin in drug development, Cardiovasc. Res. 58 (2003) 32–45.
[84] M. Dichiara, F.A. Ambrosio, C. Barbaraci, R. González-Cano, G. Costa, C. Parenti, A. Marrazzo, L. Pasquinucci, E.J. Cobos, S. Alcaro, E. Amata, Synthesis, computational insights, and evaluation of novel sigma receptors ligands, ACS Chem. Neurosci. 14 (2023) 1845–1858.
[85] V.H. Abrego, B. Martínez-Pérez, L.A. Torres, E. Angeles, L. Martínez, J. L. Marroquín-Pascual, R. Moya-Hernández, H.A. Amaro-Recillas, J.C. Rueda-Jackson, D. Rodríguez-Barrientos, A. Rojas-Hernández, Antihypertensive and antiarrhythmic properties of a para-hydroxy[bis(ortho-morpholinylmethyl)] phenyl-1,4-DHP compound: comparison with other compounds of the same kind and relationship with logP values, Eur. J. Med. Chem. 45 (2010) 4622–4630.
[86] V. Virtanen, M. Karonen, Partition coefficients (logP) of hydrolysable tannins, Molecules (2020) 25.
[87] K. Yamamoto, Y. Ikeda, Kinetic solubility and lipophilicity evaluation connecting formulation technology strategy perspective, J. Drug Deliv. Sci. Technol. 33 (2016) 13–18.